Robotica (2012) volume 30, pp. 517–535. © Cambridge University Press 2011
doi:10.1017/S0263574711000750

Feedback control framework for car-like robots using the unicycle controllers

Maciej Michałek* and Krzysztof Kozłowski

Chair of Control and Systems Engineering, Poznan University of Technology (PUT), Piotrowo 3A, 60-965 Poznań, Poland

(Accepted June 15, 2011. First published online: July 25, 2011)

SUMMARY

The paper introduces a novel general feedback control framework, which allows applying the motion controllers originally dedicated for the unicycle model to the motion task realization for the car-like kinematics. The concept is formulated for two practically meaningful motorizations: with a front-wheel driven and with a rear-wheel driven. All the three possible steering angle domains for car-like robots—limited and unlimited ones—are treated. Description of the method is complemented by the formal stability analysis of the closed-loop error dynamics. The effectiveness of the method and its limitations have been illustrated by numerous simulations conducted for the three main control tasks, namely, for trajectory tracking, path following, and set-point regulation.

KEYWORDS: Wheeled mobile robots; Kinematics; Feedback control.

1. Introduction

The most popular kinematic structures of wheeled mobile robots used in practice are the unicycle and car-like models.[17,18,20,35] Designing the feedback motion controllers has been usually done separately for the two of mentioned kinematics. Due to simplicity and the special geometrical features of the unicycle model, a lot of alternative and effective control solutions have been proposed in the literature for this kind of vehicle (from now on, we will call them the *unicycle controllers*).[1,4,6,8,11,15,19,23,24,26,27,32–34] On the other hand, the more involved problem of motion control for car-like vehicles has been treated less frequently. More often, it has been tackled utilizing an auxiliary transformed model,[28] the most often in a form of the canonical chained system.[3,20,22,23,29,31] The latter approach, although very general and elegant, may reveal some known drawbacks like locality of the chained-form transformation, and the lack of guarantee for the dynamic control quality invariance between the chained-system configuration space and the vehicle task space where the motion is realized.

Control design for the original state space of the car-like kinematics is not a trivial problem and it is more involved than for the unicycle. Both models belong to the nonholonomic underactuated systems for which the number of configuration variables is strictly greater than the number of control inputs.[10,30] Additionally, the time evolution of both systems is constrained due to the nonslip motion assumption for the vehicle wheels. An important difference between the unicycle and car-like kinematics results from the control inputs defined for them, which determine the influence on the instantaneous motion curvature of the robot platforms. The inputs for the unicycle kinematics, denoted by v_1 and v_2 in Fig. 1, are directly the angular velocity of the platform and the longitudinal velocity of the so-called *guidance point* P, respectively. As a consequence, any desired motion curvature of the unicycle can be instantaneously forced by appropriately relating the two inputs to each other. Due to the nonholonomic constraints, the instantaneous center of rotation (ICR) is constrained for the unicycle to the axle of the driving wheels. In contrast, for the car-like vehicles, the instantaneous motion curvature cannot be changed directly by varying the proportion of the available control inputs, since the first control input (denoted by u_1 in Fig. 1) is in this case the rate of the steering wheel pivoting, not the angular velocity of the robot platform. A desired motion curvature of the car-like robot can be achieved by changing the angle of the steering wheel that is related to the control input u_1 by the first-order dynamics. Thus, in this case, the motion curvature change is *delayed* due to the additional dynamics of the steering process. For the special motorization of the car-like kinematics where the rear wheel axle is driven, the motion curvature is limited to some bounded range in contrast to the unicycle (the ICR cannot be located at point P due to the kinematics singularity).

Several dedicated feedback controllers for car-like robots derived for its original configuration space have been proposed in the literature, for example,[12,16,36,38] where the rear-wheel-driven (RD) kinematics was considered, and ref. [9] treating the front-wheel-driven (FD) car-like model. The practical verification examples of selected control laws for full-size road vehicles can be found in refs. [7, 37].

The main contribution of this paper is a general, and geometrical in nature, feedback control framework for the car-like kinematics applying controllers originally dedicated for the unicycle model. It is expected that the idea will allow one to effectively control the vehicle body-posture subsystem utilizing features of the unicycle controllers widely proposed in the literature. The solution presented in this paper takes into account two types of motorizations of the car-like vehicles—with a front-wheel driven and with a rear-wheel

* Corresponding author. E-mail: maciej.michalek@put.poznan.pl

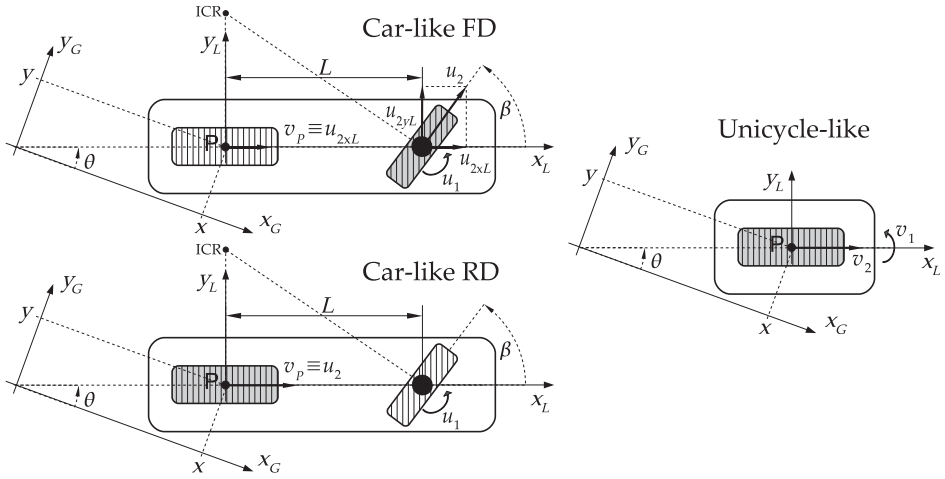

Fig. 1. Car-like mobile robots and the unicycle-like mobile robot in a global frame. Car-like robots have been presented with two kinds of motorization: FD with front-wheel driven and RD with rear-wheel driven (the wheel depicted in dark gray is directly driven by a motor).

driven.[1] All the practically possible cases for the steering angle domain, leading to the limited and unlimited robot motion curvature, are treated. The concept utilizes specific geometrical features of the car-like kinematics, which can be decomposed into two subsystems: the body posture one equivalent to the unicycle model with redefined inputs, and the steering subsystem describing the dynamics of the steering wheel. It is shown that the wide range of unicycle controllers known from the robotic literature and designed for different motion tasks can be effectively and relatively easily applied to the car-like vehicles using the framework proposed in the paper. The most important features of the presented control framework comes from its unique geometrical features where the car-like kinematic models are treated without approximations, without a need of any auxiliary state variable transformations, and where the two car-like motorizations with all practically possible steering angle domains can be treated in a unified manner. To the authors' best knowledge, any similar concept meeting all the mentioned features together has not been proposed in the literature so far.

Notation. In the paper, the following notation will be used. By $f(x,\cdot)$, one denotes function f that depends on the argument x and possibly also on some other arguments undefined at the moment and indicated by the dot mark; if one does not need or does not want to specify any arguments of the function, one simply writes $f(\cdot)$. One indicates a set of uniformly bounded m-dimensional vector functions by $\mathcal{L}_\infty^m$, by $\mathbb{R}$ the set of real numbers. The time variable is denoted by symbol τ, while the subscript t indicates the reference signals. Equality by definition is denoted by $\triangleq$, while the symbol $:=$ means *equal due to substitution*. The expression $\partial \boldsymbol{f}(\cdot)/\partial\tau$ denotes the partial derivative related only to those terms of function $\boldsymbol{f}$ that are explicitly dependent on the time variable.

[1] We consider the car-like models in their generic (minimal) form with the front and rear wheels degenerated to single wheels placed in the midpoints of particular wheel axles (see Fig. 1).

2. Problem Formulation

Consider kinematic models of the car-like mobile robot presented in Fig. 1 in two versions of motorization: FD with front-wheel driven and RD with rear-wheel driven. Assuming that the *guidance point* P is located in the center of the rear wheel, the kinematic models can be formulated in the following form:

$$\Sigma_{\mathrm{FD}}: \quad \begin{bmatrix}\dot\beta\\ \dot\theta\\ \dot x\\ \dot y\end{bmatrix} = \begin{bmatrix}1\\0\\0\\0\end{bmatrix} u_1 + \begin{bmatrix}0\\ \frac{1}{L}\sin\beta\\ \cos\beta\cos\theta\\ \cos\beta\sin\theta\end{bmatrix} u_2, \qquad (1)$$

$$\Sigma_{\mathrm{RD}}: \quad \begin{bmatrix}\dot\beta\\ \dot\theta\\ \dot x\\ \dot y\end{bmatrix} = \begin{bmatrix}1\\0\\0\\0\end{bmatrix} u_1 + \begin{bmatrix}0\\ \frac{1}{L}\tan\beta\\ \cos\theta\\ \sin\theta\end{bmatrix} u_2, \qquad (2)$$

where $L > 0$ is a distance between the front and rear wheels, $\boldsymbol{q} = [\beta\ \theta\ x\ y]^{\mathrm{T}} \in \mathcal{Q}_\beta \times \mathbb{R} \times \mathbb{R}^2$ is the configuration vector with geometrical interpretation explained in Fig. 1, and $\boldsymbol{u} = [u_1\ u_2]^{\mathrm{T}} \in \mathbb{R}^2$ is the control input with u_1 being the front-wheel steering angular velocity, and u_2 being the longitudinal velocity of the driving wheel.

The two models (1) and (2) belong to the same class of wheeled vehicles with one degree of mobility and one degree of steerability (kinematics (1,1), see ref. [10]). The ICR for both vehicle types is constrained to the rolling axle of the rear wheel and is defined by the point where it is crossed by the rolling axle of the front wheel (compare Fig. 1). The main difference between models (1) and (2) results from the way the vehicle platforms are driven by the second control input u_2. For the RD motorization, the front wheel is pushed in its admissible direction proportionally only to the projection $u_2\cos\beta$, which degenerates to zero for $|\beta| = \pi/2$. Hence, in the latter case, the kinematics (2) becomes singular because $\tan(\beta = \pm\pi/2) = \infty$ and the vehicle cannot move in any direction without slippage of the wheels (the *jamming effect*). The FD kinematics (1) does not suffer from this limitation—for $|\beta| = \pi/2$, the ICR is located at the guidance point P and the vehicle platform can rotate around this point without

limits. The similarity of the two models (1) and (2) can be easily revealed by using $u_2 \cos\beta$ as the second input in model (2) instead of u_2; in this case, both models have the same structure. Using $u_2 \cos\beta$ as the second input in Eq. (2) would indicate that one considers only this part of the rear-wheel driving velocity that pushes the front wheel along its admissible direction (direction resulting from its natural roll without slippage of the wheel).

The kinematics (1) and (2) are characterized by different configuration subspaces $\mathcal{Q}_\beta$. There are three possibilities:

C1. $\mathcal{Q}_\beta = (-\beta_m, \beta_m), \quad \beta_m = \infty, \quad (\mathcal{Q}_\beta \equiv \mathbb{R}),$
C2. $\mathcal{Q}_\beta = [-\beta_m, \beta_m], \quad \beta_m = \pi/2,$
C3. $\mathcal{Q}_\beta = [-\beta_m, \beta_m], \quad \beta_m < \pi/2,$

where $\beta_m > 0$ is the maximal steering angle value admissible for the considered model. System Σ_{FD} admits subspaces C1 to C3, while Σ_{RD} only C3 due to the model singularity obtained for $\tan\beta_m$ and $\beta_m = \pi/2$. Note that for C1 and C2, the maximal value for curvature $\kappa = \frac{1}{L}\tan\beta$ for car-like kinematics is infinite, but for the constrained case C3, it is finite and equal to $\kappa_m = \frac{1}{L}\tan\beta_m$. In case C1, one assumes free rotation of the steering wheel around a vertical axis (such a steering motorization is possible in robotic vehicles—for an exemplary steering mechanism see ref. [2]). Case C2 is simpler in practical applications and preserves the maximal motion curvature attained for C1. Case C3 has the simplest realization and is characteristic of kinematics of conventional cars and bicycles.

Models (1) and (2) describe only the kinematics (motion geometry) of the car-like vehicles with control inputs defined in the space of velocities. All the effects resulting from acceleration of the vehicle mass, rotational inertias, friction forces, actuator dynamics, and other dynamical effects are neglected here according to the implicit assumption about the presence of the cascaded control system, in which the inner velocity loops decouple the outer (kinematic-level) control loop from all the mentioned dynamic effects. In this case, treating the kinematics as the representative models of the considered vehicles seems to be practically justified and useful.[2] In the cascaded control system, the control inputs computed on the kinematic level are treated as the desired velocities, which should be achieved using regulators in the inner loops on the basic control level. From now on, our attention will be focused on the kinematic level of the whole control system.

In most practical motion tasks, the body-posture configuration $\overline{\boldsymbol{q}} = [\theta \ x \ y]^{\mathrm{T}}$ of models (1) and (2) is more relevant than the steering wheel configuration represented by β. By properly redefining the control input $\boldsymbol{u}$, it is possible to rewrite the body-posture subsystem of Σ_{FD} and Σ_{RD} in the form of unicycle kinematics with configuration vector $\overline{\boldsymbol{q}} \in \mathbb{R}^3$ and new input $\boldsymbol{v} \in \mathbb{R}^2$. The problem considered in this paper is to formulate the general framework allowing a user to apply the feedback controllers originally dedicated to unicycle kinematics to the car-like kinematics (1) or (2) in order to control its body-posture configuration $\overline{\boldsymbol{q}}$.

[2] It is worth noting that the essential difficulties with control design for nonholonomic wheeled robots are related to the kinematics (motion geometry), not to the dynamics of the vehicle.

To make our considerations strict enough, let us recall the unicycle kinematics

$$\begin{bmatrix} \dot\theta \\ \dot x \\ \dot y \end{bmatrix} = \begin{bmatrix} 1 & 0 \\ 0 & \cos\theta \\ 0 & \sin\theta \end{bmatrix} \begin{bmatrix} v_1 \\ v_2 \end{bmatrix} \Rightarrow \dot{\overline{\boldsymbol{q}}} = \overline{\boldsymbol{G}}(\overline{\boldsymbol{q}})\boldsymbol{v} \tag{3}$$

with the configuration $\overline{\boldsymbol{q}} = [\theta \ x \ y]^{\mathrm{T}} \in \mathbb{R}^3$ and with the input vector $\boldsymbol{v} = [v_1 \ v_2]^{\mathrm{T}} \in \mathbb{R}^2$, where v_1 is a vehicle angular velocity, and v_2 is a longitudinal velocity of its guidance point P (compare Fig. 1). We assume for the kinematics (3) that the original bounded feedback control function is given by

$$\boldsymbol{\phi}(\overline{\boldsymbol{e}}(\tau), \cdot) = \begin{bmatrix} \phi_1(\overline{\boldsymbol{e}}(\tau), \cdot) \\ \phi_2(\overline{\boldsymbol{e}}(\tau), \cdot) \end{bmatrix} \in \mathcal{L}^2_\infty, \tag{4}$$

where

$$\overline{\boldsymbol{e}} = \begin{bmatrix} e_\theta & e_x & e_y \end{bmatrix}^{\mathrm{T}} \triangleq (\overline{\boldsymbol{q}}_t - \overline{\boldsymbol{q}}) \in \mathbb{R}^3 \tag{5}$$

is a posture error, $\overline{\boldsymbol{q}}_t = [\theta_t \ \ x_t \ \ y_t]^{\mathrm{T}} \in \mathbb{R}^3$ is a bounded reference posture-trajectory, and $\tau \in \mathbb{R}_{\geq 0}$ is a time variable. Assume also that Eq. (4) is an asymptotic stabilizer meaning that after its application to kinematics (3) by taking $\boldsymbol{v} := \boldsymbol{\phi}(\overline{\boldsymbol{e}}(\tau), \cdot)$ it is ensured that $\lim_{\tau\to\infty} \|\overline{\boldsymbol{e}}(\tau)\| = 0$ uniformly in time. We additionally restrict the time-varying reference configurations $\overline{\boldsymbol{q}}_t(\tau)$ and control function $\boldsymbol{\phi}(\cdot)$ in Eq. (4) as follows:

A1. $\overline{\boldsymbol{q}}_t(\tau) \in C^d$ is an *admissible* trajectory satisfying Eq. (3) with d sufficiently high,
A2. $\forall\, \tau \geq 0 \quad \left|\frac{v_{1t}(\tau)}{v_{2t}(\tau)}\right| = \left|\frac{\dot\theta_t(\tau)}{\dot x_t(\tau)\cos\theta_t(\tau) + \dot y_t(\tau)\sin\theta_t(\tau)}\right| \leq \left|\frac{\tan\beta_m}{L}\right|,$
A3. $\partial\boldsymbol{\phi}_{1,2}/\partial\overline{\boldsymbol{e}} \in \mathcal{L}^3_\infty, \ \partial\boldsymbol{\phi}/\partial\tau \in \mathcal{L}^2_\infty,$
A4. $|\phi_1(\tau)/\phi_2(\tau)| \leq \left|\frac{1}{L}\tan\beta_m\right|$ for almost all $\tau \geq 0,$

where $v_{1t}(\tau)$ and $v_{2t}(\tau)$ are the reference inputs (velocities) for the unicycle. The problem considered in the paper can be formulated as follows.

Problem 1 *The problem is to find feedback control laws* $\boldsymbol{u} = \boldsymbol{u}(\boldsymbol{\phi}, \boldsymbol{q}, \cdot)$, *which—when applied to car-like kinematics (1) or (2)—guarantee that the time evolution of their body-posture configuration* $\overline{\boldsymbol{q}}$ *will be determined (at least asymptotically) by Eq. (3) with input* $\boldsymbol{v} := \boldsymbol{\phi}(\overline{\boldsymbol{e}}(\tau), \cdot)$ *under assumptions A1–A4.*

Let us shortly justify and comment on restrictions imposed by A1–A4. The continuity of the reference trajectory $\overline{\boldsymbol{q}}_t(\tau)$ in A1 is necessary to ensure the boundedness of the original control law (4) in the sense of these terms where the time derivatives of reference signals are utilized. The order d (smoothness order) in A1 depends on the particular form of the original control function selected in Eq. (4). The admissibility introduced in assumption A1 means that the reference trajectory $\overline{\boldsymbol{q}}_t(\tau)$ is feasible for the original unicycle model by preserving its nonholonomic constraints imposed by Eq. (3). The admissibility is a necessary condition to obtain the asymptotic convergence in the closed-loop system (3)+(4).[21,22] Since we assume that Eq. (4) is an asymptotic stabilizer for the unicycle, the reference signals must satisfy the admissibility condition stated in A1. The assumption

of boundedness for partial derivatives imposed in A3 is important to ensure the boundedness of time derivatives $\dot{\phi}_1$ and $\dot{\phi}_2$ used further in the proposed control strategy (see Eqs. (16) and (17)). A2 and A4 determine the motion feasibility assumptions for the car-like kinematics in the sense of the maximal motion curvature the vehicle can attain. They result from the fact that not all instantaneous motion curvatures can be physically realized by car-like kinematics constrained by the limited steering configuration given by C3. Assumption A2 imposes the upper limit for the instantaneous motion curvature defined by the unicycle reference trajectory (on the right-hand side in the inequality). This reference curvature should satisfy the upper bound of the robot curvature resulting from the maximal steering angle value β_m achievable by the car-like vehicle. Thus, A2 maps the motion curvature feasibility of the car-like vehicle into the set of admissible reference trajectories of the reference unicycle. Note that the inequality in A2 is only limiting if $|\beta_m| < \pi/2$. Similarly, assumption A4 maps the motion curvature feasibility of the car-like vehicle into the set of admissible feedback control actions $\boldsymbol{\phi}(\tau)$ originally designed for the unicycle. Thus, only the control actions of Eq. (4) that satisfy A4 can be successfully emulated by the car-like vehicle. To make A4 less restrictive in practice, one admits its violation in a zero-measure set of time instants during a transient stage, when A4 may be temporarily not met. Apart from some modification of the transients, this temporal violation will not have any degrading consequences asymptotically, since according to A2 the inequality in A4 is satisfied in a sufficiently small vicinity of $\overline{\boldsymbol{q}}_t(\tau)$ and along $\overline{\boldsymbol{q}}_t(\tau)$.

According to Problem 1 and the assumptions formulated above the aim is to emulate the time evolution of the closed-loop system (3)+(4) by the body-configuration vector $\overline{\boldsymbol{q}}$ of the car-like kinematics in order to preserve the convergence results originally proved for the unicycle when controlled by the stabilizer (4). A solution to Problem 1 for the two car-like kinematics Σ_{FD} and Σ_{RD}, taking into account all the three cases of steering subspaces given by C1 to C3, will be proposed in the sequel.

3. Applying the Unicycle Controllers to Car-Like Kinematics

The concept proposed in the paper can be generally described as follows. First, we redefine the input signals to original kinematics (1) and (2) using an invertible transformation $\boldsymbol{f}_u : (u_2, \beta) \mapsto \boldsymbol{v}$ to obtain the car-like model in a form of concatenation of the body-posture subsystem in the unicycle form with new inputs $\boldsymbol{v}$, and the remaining steering dynamics $\dot{\beta} = u_1$ (the first rows of Eqs. (1) and (2))

$$\dot{\beta} = u_1, \tag{6}$$

$$\dot{\overline{\boldsymbol{q}}} = \overline{\boldsymbol{G}}(\overline{\boldsymbol{q}})\boldsymbol{v}, \tag{7}$$

where Eq. (7) has the unicycle-like structure defined in Eq. (3). Second, for the *nominal* control functions $\boldsymbol{\phi}$ taken from the selected unicycle controller (and substituted into $\boldsymbol{v}$ according to Eq. (4)), we have to recover the original input u_2 and a desired steering angle β_d using the inverse transformation: $(u_2(\boldsymbol{\phi}), \beta_d(\boldsymbol{\phi})) = \boldsymbol{f}_u^{-1}(\boldsymbol{\phi})$. Note that we have to use here the *desired* angle β_d instead of β since the steering angle and input u_1 in the car-like kinematics (1) and (2) are related to each other by the integral relation (additional dynamics for the steering variable). Now, the pair $(u_2(\boldsymbol{\phi}), \beta_d(\boldsymbol{\phi}))$ denotes the desired driving velocity and the desired steering angle, which—if realized precisely—guarantee that $\boldsymbol{v} := \boldsymbol{f}_u(u_2(\boldsymbol{\phi}), \beta_d(\boldsymbol{\phi})) = \boldsymbol{\phi}$. The latter equation implies that the body-posture subsystem of the original car-like kinematics is driven by the control functions $\boldsymbol{\phi}$ determined by the unicycle controller; thus, time evolution of the body-posture subsystem is fully determined by Eqs. (3) and (4). Third, since the steering angle β cannot be forced directly to β_d (compare first rows of Eqs. (1) and (2)), introduction of the steering angle stabilizing controller $u_1 = u_1(\beta_d(\boldsymbol{\phi}), \beta, \cdot)$ guaranteeing that $\beta \to \beta_d$ is required in the last design stage. Details of the design stages mentioned above specialized to both car-like models—FD and RD—are described below.

Let us first consider the car-like model with FD motorization. Introducing the new control inputs

$$\boldsymbol{f}_u^{\mathrm{FD}} : \quad v_1 := \frac{1}{L} u_2 \sin\beta, \quad v_2 := u_2 \cos\beta \tag{8}$$

for the body-posture subsystem of Σ_{FD} allows rewriting Eq. (1) in the form of two subsystems denoted by Eqs. (6) and (7). By substituting $v_1 = \phi_1$ and $v_2 = \phi_2$, the inverse transformation $(\boldsymbol{f}_u^{\mathrm{FD}})^{-1}$ leading to the pair $(u_2(\boldsymbol{\phi}), \beta_d(\boldsymbol{\phi}))$ can be easily derived according to the following relations obtained from Eq. (8):

$$u_2(\boldsymbol{\phi}) = \phi_2 \cos\beta + L\phi_1 \sin\beta, \tag{9}$$

$$\tan\beta = \frac{L\phi_1 \cdot u_2}{\phi_2 \cdot u_2}. \tag{10}$$

Equation (9) finally determines the driving control function for kinematics (1). On the other hand, relation (10) cannot be met instantaneously because the steering angle β is related to the control input u_1 through the integral relation according to Eq. (1). Hence, in order to meet Eq. (10), one proposes to introduce the auxiliary desired steering variable

$$\beta_d(\boldsymbol{\phi}) \triangleq \begin{cases} \mathrm{Atan2c}(\gamma L\phi_1, \gamma\phi_2) & \text{for C1,} \\ \mathrm{Sat}(\arctan(L\phi_1/\phi_2), \beta_m) & \text{for C2, C3,} \end{cases} \tag{11}$$

where $\gamma \triangleq \mathrm{sgn}(u_2(\boldsymbol{\phi})) \in \{-1, +1\}$, $\mathrm{Atan2c}(\cdot,\cdot) : \mathbb{R} \times \mathbb{R} \mapsto \mathbb{R}$ is a continuous version[3] of the four-quadrant function $\mathrm{Atan2}(\cdot,\cdot) : \mathbb{R} \times \mathbb{R} \mapsto (-\pi, \pi]$, and

$$\mathrm{Sat}(f, B) \triangleq \begin{cases} f & \text{if } |f| \le B, \\ B\,\mathrm{sgn}(f) & \text{if } |f| > B. \end{cases} \tag{12}$$

In order to preserve the original domain of the steering angle definition $\mathcal{Q}_\beta$, the maximum steering angle value β_m

[3] More details on computations of $\mathrm{Atan2c}(\cdot,\cdot)$ can be found in ref. [19].

in Eq. (11) should be appropriately chosen according to the configuration subspace under consideration (see C2 and C3). To guarantee that β is convergent to $\beta_d(\boldsymbol{\phi})$ (and, as a consequence, Eq. (10) is met), we define the steering error

$$e_d \triangleq \beta_d(\boldsymbol{\phi}) - \beta, \tag{13}$$

which should be made convergent to zero using the input u_1. Let us propose the steering angle stabilizer in the form of

$$u_1(e_d, \cdot) \triangleq k_d \operatorname{sgn}(e_d) |e_d|^{\delta} + \dot{\beta}_d(\boldsymbol{\phi}), \tag{14}$$

with $k_d > 0$ and $\delta \in (0, 1]$ treated as design parameters (for explanation see Remark 1). The term $\dot{\beta}_d(\boldsymbol{\phi})$ in Eq. (14) results from the time derivative of Eq. (11)

$$\dot{\beta}_d(\boldsymbol{\phi}) = \begin{cases} \frac{L(\dot{\phi}_1\phi_2 - \phi_1\dot{\phi}_2)}{L^2\phi_1^2 + \phi_2^2} & \text{if } |\beta_d(\boldsymbol{\phi})| \le \beta_m, \\ 0 & \text{if } |\beta_d(\boldsymbol{\phi})| > \beta_m, \end{cases} \tag{15}$$

where

$$\dot{\phi}_1 = \frac{\partial \phi_1}{\partial \overline{\boldsymbol{e}}}\dot{\overline{\boldsymbol{e}}} + \frac{\partial \phi_1}{\partial \tau} \overset{(7)}{=} \frac{\partial \phi_1}{\partial \overline{\boldsymbol{e}}}\left(\dot{\overline{\boldsymbol{q}}}_t - \overline{\boldsymbol{G}}(\overline{\boldsymbol{q}})\boldsymbol{v}\right) + \frac{\partial \phi_1}{\partial \tau}, \tag{16}$$

$$\dot{\phi}_2 = \frac{\partial \phi_2}{\partial \overline{\boldsymbol{e}}}\dot{\overline{\boldsymbol{e}}} + \frac{\partial \phi_2}{\partial \tau} \overset{(7)}{=} \frac{\partial \phi_2}{\partial \overline{\boldsymbol{e}}}\left(\dot{\overline{\boldsymbol{q}}}_t - \overline{\boldsymbol{G}}(\overline{\boldsymbol{q}})\boldsymbol{v}\right) + \frac{\partial \phi_2}{\partial \tau}. \tag{17}$$

The particular form of the above derivatives depends on the unicycle controller selected by a user.

To obtain the Σ_{RD} model in the form of Eqs. (6) and (7), we redefine the inputs to the body-posture kinematics of Eq. (2) as

$$\boldsymbol{f}_u^{\mathrm{RD}}: \quad v_1 := \frac{1}{L} u_2 \tan\beta, \qquad v_2 := u_2. \tag{18}$$

After substituting $v_1 = \phi_1$ and $v_2 = \phi_2$, the inverse transformation $(\boldsymbol{f}_u^{\mathrm{RD}})^{-1}$ leading to the pair $(u_2(\boldsymbol{\phi}), \beta_d(\boldsymbol{\phi}))$ can be derived according to the following relations obtained from Eq. (18):

$$u_2(\boldsymbol{\phi}) = \cos\beta(\phi_2 \cos\beta + L\phi_1 \sin\beta), \tag{19}$$

$$\tan\beta = \frac{L\phi_1}{\phi_2}. \tag{20}$$

Equation (19) determines the final driving control function for kinematics (2). Again Eq. (20) cannot be met instantaneously due to the integral relation between angle β and the input u_1 in Eq. (2). Hence, one introduces the auxiliary desired steering variable

$$\beta_d(\boldsymbol{\phi}) \triangleq \mathrm{Sat}(\arctan(L\phi_1/\phi_2), \beta_m), \tag{21}$$

with $\mathrm{Sat}(\cdot, \cdot)$ determined in Eq. (12). Note that due to the structural singularity of the RD kinematics, definition (21) is now valid only for the steering configuration subspace defined by C3 ($\beta_m < \pi/2$). Now, we proceed similarly as for the FD motorization recalling the steering error (13), computed in this case for Eq. (21), and the steering angle stabilizer (14) with the feed-forward term given by Eq. (15) and time derivatives (16) and (17). Using these definitions, one finishes the last general control design stage for RD kinematics.

Remark 1 *The steering angle stabilizer introduced in Eq. (14) has a flexible structure that allows the designer to select type of convergence for the steering error $e_d(\tau)$: either infinite time or finite time. By taking $\delta = 1$, the stabilizer (14) simplifies to the linear controller $u_1 = k_d\, e_d + \dot{\beta}_d(\boldsymbol{\phi})$, which guarantees asymptotic (infinite time) convergence of $e_d(\tau)$. By taking δ in the range $(0, 1)$, one obtains a finite-time continuous (but non-Lipschitz at zero) stabilizer that makes the error $e_d(\tau)$ tend to zero within a finite time horizon.[5] Selection of the exponent δ in this case influences the convergence duration for e_d according to the strategy: the less the exponent value the shorter the convergence time. For justification of the above claims, the reader is referred to the formal analysis in Section 3.1.*

The block schema explaining the computational flowchart of the proposed control framework is shown in Fig. 2. The reference generator block and the underlying control law are directly applied here as for the unicycle kinematics. Adopting the unicycle control strategy to a vehicle body of the car-like vehicle is possible thanks to the intermediate block denoted in Fig. 2 by a gray box. For the computations of time derivative $\dot{\boldsymbol{\phi}} = [\dot{\phi}_1\ \dot{\phi}_2]^{\mathrm{T}}$ (compare Eqs. (16) and (17)), one can use the redefined input $\boldsymbol{v} = [v_1\ v_2]^{\mathrm{T}}$ determined upon the current values of u_2 and β following Eq. (8) or Eq. (18). Note that the body configuration $\overline{\boldsymbol{q}}$ is an output of the controlled *process*, while steering angle β is treated here as an auxiliary (internal) variable.

Remark 2 *Definitions (11), (15), and (21) are not determined at time instants $\overline{\tau}$ when $\phi_1(\overline{\tau}) = \phi_2(\overline{\tau}) = 0$. For time-varying reference configurations $\overline{\boldsymbol{q}}_t(\tau)$, it may occasionally occur during a transient stage, but it cannot be persistent since the control function $\boldsymbol{\phi}(\cdot)$ if asymptotically stabilizing from assumption. If the body-configuration reference $\overline{\boldsymbol{q}}_t$ is constant, the only possibility for time-invariant stabilizers is $\boldsymbol{\phi}(\overline{\boldsymbol{e}}, \tau) = \boldsymbol{0}$ for $\overline{\boldsymbol{e}} = \boldsymbol{0}$, again due to the assumed asymptotic stabilizing feature of $\boldsymbol{\phi}(\cdot)$ and driftless nature of kinematics (3). In this case, condition $\boldsymbol{\phi}(\overline{\boldsymbol{e}} = \boldsymbol{0}, \tau) = \boldsymbol{0}$ cannot be valid in finite time from assumption ($\boldsymbol{\phi}(\cdot)$ is not a finite-time stabilizer) if $\|\overline{\boldsymbol{e}}(0)\| \neq 0$; therefore, it is theoretically avoidable. However, in cases where either $\overline{\boldsymbol{q}}_t$ is time varying or if $\overline{\boldsymbol{q}}_t$ is constant but $\|\overline{\boldsymbol{e}}(0)\| = 0$ or the selected set-point stabilizer is time varying, one needs to cope with the indeterminacy mentioned above. Hence, to obtain the controller well determined for these cases, we propose to introduce additional definitions for the desired steering angle and its time derivative*

$$\beta_d(\boldsymbol{\phi}(\overline{\tau})) \triangleq \beta_d(\boldsymbol{\phi}(\overline{\tau}_-)) = \lim_{\tau \to \overline{\tau}_-} \beta_d(\boldsymbol{\phi}(\tau)), \tag{22}$$

$$\dot{\beta}_d(\boldsymbol{\phi}(\overline{\tau})) \triangleq 0, \tag{23}$$

if the limit in Eq. (22) exists, or

$$\beta_d(\boldsymbol{\phi}(\overline{\tau})) \triangleq 0, \qquad \dot{\beta}_d(\boldsymbol{\phi}(\overline{\tau})) \triangleq 0 \tag{24}$$

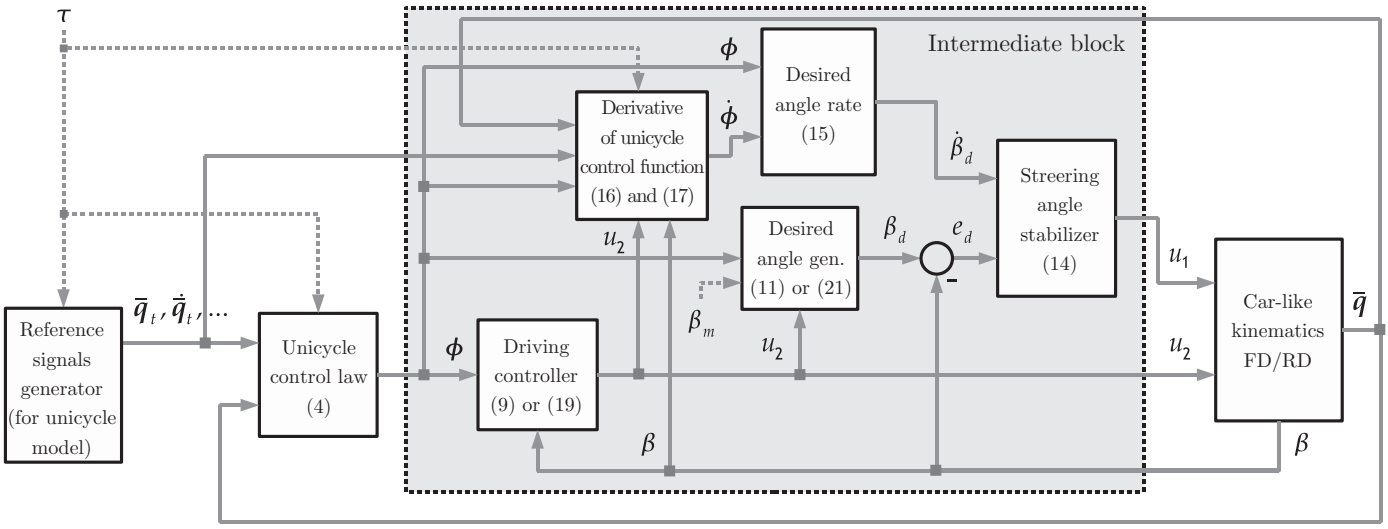

Fig. 2. Block schema of the general control framework, which allows applying unicycle controllers to the car-like kinematics.

in the opposite case. The above definitions can be used for $\|\boldsymbol{\phi}(\bar{\tau})\| = 0$ *or for* $\|\boldsymbol{\phi}(\tau)\| < \varepsilon$, *where* $\varepsilon > 0$ *is an assumed sufficiently small vicinity of the indeterminacy point. The latter condition utilized together with the switching* $u_2(\|\boldsymbol{\phi}(\tau)\| < \varepsilon) := 0$ *may be preferred in practical applications attenuating the negative influence of the measurement noise or a finite numerical precision in particular control implementation.*

Remark 3 *For the RD motorization, one can formulate an alternative definition for the desired steering angle* β_d *instead of Eq. (21). Using only the first equation of Eq. (18), one can propose*

$$\beta_d(\boldsymbol{\phi}) \triangleq \mathrm{Sat}(\arctan(L\phi_1/u_2(\boldsymbol{\phi})), \beta_m) \tag{25}$$

with $u_2(\boldsymbol{\phi})$ *taken from Eq. (19). In practice, definition (25) may reveal some benefits over Eq. (21). Namely, since for RD kinematics the driving input given by Eq. (19) can be equal to zero when simultaneously* $\phi_1 = \phi_2 = 0$, *the saturation of Eq. (25) obtained for division by zero in* $\arctan(\cdot)$ *function may occur less frequent than in Eq. (21).*

3.1. Stability analysis

To analyze stability of the proposed closed-loop control system for FD and RD car-like robots, one needs to take into account the reformulated kinematics represented by Eqs. (6) and (7) together with the steering stabilizing controller (14) and body-posture inputs determined, as appropriate, by Eq. (8) or Eq. (18) with driving control u_2 given by Eq. (9) or Eq. (19), respectively. We need to check the boundedness and convergence properties of body-posture error $\bar{\boldsymbol{e}}(\tau)$, and the time behavior of steering angle $\beta(\tau)$. First, we consider the case when $\phi_1^2 + \phi_2^2 \neq 0$, thus definitions (11), (15), and (21) are well determined.

We start with applying the steering control (14) to subsystem (6), which gives a differential equation in the form

$$\dot{e}_d = -k_d \,\mathrm{sgn}(e_d)\,|e_d|^{\delta} \triangleq f_d(e_d). \tag{26}$$

For $\delta = 1$, the solution of Eq. (26) is asymptotically stable

$$\lim_{\tau\to\infty} e_d(\tau) = 0, \qquad e_d(\tau) = e_d(0)\exp(-k_d\tau), \tag{27}$$

while for $\delta \in (0, 1)$ one obtains the finite-time convergence (see ref. [5])

$$\lim_{\tau\to T_d} e_d(\tau) = 0, \quad T_d = \frac{2V_{d0}^{(1-\delta)/2}}{c_d(1-\delta)}, \tag{28}$$

where $c_d = k_d\sqrt{2}^{\delta+1}$, $V_{d0} = \frac{1}{2}e_d^2(0)$. The above convergence results will be used in the sequel.

Since the original feedback control function $\boldsymbol{\phi}(\cdot)$ given in Eq. (4) is assumed to be bounded, one can define its upper bound

$$\phi_m = \sup_{\tau\geq 0} \|\boldsymbol{\phi}(\bar{\boldsymbol{e}}(\tau), \tau)\| < \infty. \tag{29}$$

For the *nominal* case, $\boldsymbol{v} = \boldsymbol{\phi}(\cdot)$ is an asymptotically stabilizing function for Eq. (3). Thus, using Eqs. (5) and (4), one obtains

$$\dot{\bar{\boldsymbol{e}}} = \boldsymbol{f}_n(\bar{\boldsymbol{e}}, \tau), \quad \boldsymbol{f}_n(\bar{\boldsymbol{e}}, \tau) = \dot{\bar{\boldsymbol{q}}}_t - \overline{\boldsymbol{G}}(\bar{\boldsymbol{q}}_t - \bar{\boldsymbol{e}})\boldsymbol{\phi}(\bar{\boldsymbol{e}}, \tau). \tag{30}$$

Application of the converse Lyapunov theorem (see ref. [14], Theorem 4.16) implies that for the nominal closed-loop error dynamics (30) there exists a positive definite function

$$V(\bar{\boldsymbol{e}} \neq \boldsymbol{0}, \tau) > 0, \quad V(\bar{\boldsymbol{e}} = \boldsymbol{0}, \tau) = 0, \quad \forall\,\tau \geq 0, \tag{31}$$

which meets the following relations:

$$\rho_1(\|\bar{\boldsymbol{e}}\|) \leq V(\bar{\boldsymbol{e}}, \tau) \leq \rho_2(\|\bar{\boldsymbol{e}}\|), \tag{32}$$

$$\dot{V}(\bar{\boldsymbol{e}}, \tau) = \frac{\partial V}{\partial \tau} + \frac{\partial V}{\partial \bar{\boldsymbol{e}}}\boldsymbol{f}_n(\bar{\boldsymbol{e}}, \tau) \leq -\rho_3(\|\bar{\boldsymbol{e}}\|), \tag{33}$$

$$\left\| \frac{\partial V}{\partial \bar{\boldsymbol{e}}} \right\| \leq \rho_4(\|\bar{\boldsymbol{e}}\|), \tag{34}$$

where $\rho_i(\cdot),\ i = 1, \ldots, 4$ are functions of class $\mathcal{K}$.

For the purpose of further considerations, let us note that the body-posture inputs $\boldsymbol{v}$ with u_2 given by Eq. (9) or Eq. (19) satisfy, for FD as well as for RD kinematics, the following equation (see Appendix):

$$\boldsymbol{v} = \begin{bmatrix} v_1 \\ v_2 \end{bmatrix} = \boldsymbol{\phi} + \boldsymbol{F}(e_d, \beta_d(\boldsymbol{\phi}))\boldsymbol{\phi} = \boldsymbol{\phi} + \boldsymbol{\epsilon}(e_d, \boldsymbol{\phi}), \tag{35}$$

where $\boldsymbol{\epsilon}(e_d = 0, \boldsymbol{\phi}) = \boldsymbol{0}$ can be treated as an input-additive vanishing perturbation, $\boldsymbol{\phi}(\cdot)$ is a nominal stabilizing control function introduced in Eq. (4), and

$$\boldsymbol{F}(e_d, \beta_d(\boldsymbol{\phi})) = \begin{bmatrix} -\mathrm{c}^2(\beta_d(\boldsymbol{\phi}) - e_d) & \frac{1}{L}\mathrm{s}(\beta_d(\boldsymbol{\phi}) - e_d)\mathrm{c}(\beta_d(\boldsymbol{\phi}) - e_d) \\ L\mathrm{s}(\beta_d(\boldsymbol{\phi}) - e_d)\mathrm{c}(\beta_d(\boldsymbol{\phi}) - e_d) & -\mathrm{s}^2(\beta_d(\boldsymbol{\phi}) - e_d) \end{bmatrix}. \tag{36}$$

Hereafter, Eq. (35) will be treated as a *practical* case of the control input $\boldsymbol{v}$ for the body-posture subsystem (7). For the *practical* case, by applying Eq. (35) into Eq. (7) and using Eq. (5), the closed-loop error dynamics takes the following form:

$$\dot{\overline{\boldsymbol{e}}} = \boldsymbol{f}_n(\overline{\boldsymbol{e}}, \tau) + \boldsymbol{g}(\overline{\boldsymbol{e}}, \tau, e_d) \triangleq \boldsymbol{f}(\overline{\boldsymbol{e}}, \tau, e_d), \tag{37}$$

where $\boldsymbol{f}_n(\overline{\boldsymbol{e}}, \tau)$ is defined in Eq. (30), and

$$\boldsymbol{g}(\overline{\boldsymbol{e}}, \tau, e_d) = -\overline{\boldsymbol{G}}(\overline{\boldsymbol{q}}_t - \overline{\boldsymbol{e}})\boldsymbol{\epsilon}(e_d, \boldsymbol{\phi}(\overline{\boldsymbol{e}}, \tau)) \tag{38}$$

is now an interconnection term between the body-posture error dynamics (37) and the steering error dynamics given by Eq. (26). According to Eq. (38) and since $\boldsymbol{\epsilon}(e_d = 0, \boldsymbol{\phi}) = \boldsymbol{0}$ (see Appendix), one obtains

$$\boldsymbol{g}(\overline{\boldsymbol{e}}, \tau, 0) = 0. \tag{39}$$

In function $\boldsymbol{f}(\overline{\boldsymbol{e}}, \tau, e_d)$ from Eq. (37) only component $\boldsymbol{g}(\overline{\boldsymbol{e}}, \tau, e_d)$ depends on error e_d through term $\boldsymbol{\epsilon}(e_d, \boldsymbol{\phi}(\overline{\boldsymbol{e}}, \tau)) = \boldsymbol{F}(e_d, \beta_d(\boldsymbol{\phi}))\boldsymbol{\phi}$ (see Eqs. (35) and (38)) with matrix $\boldsymbol{F}(e_d, \beta_d(\boldsymbol{\phi}))$ determined in Eq. (36). Hence, it is clear that term $\boldsymbol{g}(\overline{\boldsymbol{e}}, \tau, e_d)$ and, in a consequence, function $\boldsymbol{f}(\overline{\boldsymbol{e}}, \tau, e_d)$ from Eq. (37) is Lipschitz continuous in e_d yielding $\| \boldsymbol{f}(\overline{\boldsymbol{e}}, \tau, e_d) - \boldsymbol{f}(\overline{\boldsymbol{e}}, \tau, 0)\| \leq l\,|e_d|$, where $l > 0$ is a Lipschitz constant. Now, according to Eqs. (37) and (39), one obtains

$$\| \boldsymbol{g}(\overline{\boldsymbol{e}}, \tau, e_d)\| \leq l\,|e_d|\,. \tag{40}$$

Using inequalities (33), (34), and (40), one can asses the time derivative of the positive definite function (31) along solutions of the closed-loop dynamics (37) as follows:

$$\begin{aligned} \dot{V} &= \frac{\partial V}{\partial \tau} + \frac{\partial V}{\partial \overline{\boldsymbol{e}}}\left(\boldsymbol{f}_n(\overline{\boldsymbol{e}}, \tau) + \boldsymbol{g}(\overline{\boldsymbol{e}}, \tau, e_d)\right) \\ &= \frac{\partial V}{\partial \tau} + \frac{\partial V}{\partial \overline{\boldsymbol{e}}}\boldsymbol{f}_n(\overline{\boldsymbol{e}}, \tau) + \frac{\partial V}{\partial \overline{\boldsymbol{e}}}\boldsymbol{g}(\overline{\boldsymbol{e}}, \tau, e_d) \\ &\leq -\rho_3(\| \overline{\boldsymbol{e}}\|) + \frac{\partial V}{\partial \overline{\boldsymbol{e}}}\boldsymbol{g}(\overline{\boldsymbol{e}}, \tau, e_d) \\ &\leq -\rho_3(\| \overline{\boldsymbol{e}}\|) + \left\| \frac{\partial V}{\partial \overline{\boldsymbol{e}}} \right\| \| \boldsymbol{g}(\overline{\boldsymbol{e}}, \tau, e_d)\| \\ &\leq -\rho_3(\| \overline{\boldsymbol{e}}\|) + l\rho_4(\| \overline{\boldsymbol{e}}\|)\,|e_d| \\ &= -(1 - \chi)\rho_3(\| \overline{\boldsymbol{e}}\|) - \chi\rho_3(\| \overline{\boldsymbol{e}}\|) + l\rho_4(\| \overline{\boldsymbol{e}}\|)\,|e_d|\,, \end{aligned} \tag{41}$$

where $\chi \in (0, 1)$ is a constant. The right-hand side of Eq. (41) is negative definite for

$$\frac{\rho_3(\| \overline{\boldsymbol{e}}\|)}{\rho_4(\| \overline{\boldsymbol{e}}\|)} \geq \frac{l\,|e_d|}{\chi}. \tag{42}$$

Since $e_d(\tau)$ can tend to zero arbitrarily fast (compare Eqs. (27) and (28)), and $\rho_3(\cdot)$, $\rho_4(\cdot)$ are positive definite and strictly increasing, the inequality (42) can be met for some finite $\| \overline{\boldsymbol{e}}\| \neq 0$. Applying now Theorem 4.19 formulated in ref. [14], one can conclude about the input-to-state stability of dynamics (37) with *input* e_d. If the nominal stabilizing function $\boldsymbol{\phi}(\cdot)$ guarantees uniform exponential stability of the dynamics (30), then the bounding functions from Eqs. (33) and (34) take the form $\rho_3(\| \overline{\boldsymbol{e}}\|) = c_3 \| \overline{\boldsymbol{e}}\|^2$ and $\rho_4(\| \overline{\boldsymbol{e}}\|) = c_4 \| \overline{\boldsymbol{e}}\|$ with $c_3, c_4 > 0$ (see ref. [14], Theorem 4.14). In this case, inequality (42) leads to the explicit condition $\| \overline{\boldsymbol{e}}\| \geq (lc_4/(\chi c_3))\,|e_d|$, for which the time derivative $\dot{V}$ is negative definite implying input-to-state stability of Eq. (37).

Rewriting now the two interconnected error subsystems (37) and (26) as

$$\begin{aligned} \dot{\overline{\boldsymbol{e}}} &= \boldsymbol{f}(\overline{\boldsymbol{e}}, \tau, e_d), \\ \dot{e}_d &= f_d(e_d), \end{aligned}$$

one can recall what follows. The latter subsystem[4] has a bounded solution and the asymptotically stable equilibrium at $e_d = 0$. The first subsystem is input-to-state stable with e_d viewed as an input. For the nominal case where $\boldsymbol{v} = \boldsymbol{\phi}(\cdot)$, the error dynamics $\dot{\overline{\boldsymbol{e}}} = \boldsymbol{f}(\overline{\boldsymbol{e}}, \tau, 0) = \boldsymbol{f}_n(\overline{\boldsymbol{e}}, \tau)$ has a uniformly asymptotically stable equilibrium $\overline{\boldsymbol{e}} = \boldsymbol{0}$ by assumption. As a consequence of Lemma 4.7 given in ref. [14], one concludes that the equilibrium $[\overline{\boldsymbol{e}}^{\mathrm{T}}\ e_d]^{\mathrm{T}} = [\boldsymbol{0}\,0]^{\mathrm{T}}$ for the cascade systems (26)–(37) is uniformly asymptotically stable.

Since $e_d(\tau)$ tends to zero, the steering variable $\beta(\tau)$ is convergent to the desired steering function $\beta_d(\tau)$. To show what happens with $\beta(\tau)$ for $\overline{\boldsymbol{e}}(\tau) \to \boldsymbol{0}$, one has to analyze the time behavior of $\beta_d(\boldsymbol{\phi}(\overline{\boldsymbol{e}}, \tau))$ at this limit. We consider separately two cases: of a time-varying reference $\overline{\boldsymbol{q}}_t(\tau)$ and of a constant reference $\overline{\boldsymbol{q}}_t$.

For the case of admissible reference trajectory $\overline{\boldsymbol{q}}_t(\tau)$, it is necessary that $\boldsymbol{\phi}(\overline{\boldsymbol{e}} = \boldsymbol{0}, \tau) = \boldsymbol{v}_t(\tau)$, where the reference input $\boldsymbol{v}_t(\tau) = [\dot{\theta}_t(\tau) \quad \dot{x}_t(\tau)\cos\theta_t(\tau) + \dot{y}_t(\tau)\sin\theta_t(\tau)]^{\mathrm{T}} = [v_{1t}(\tau)\ v_{2t}(\tau)]^{\mathrm{T}}$ together with $\overline{\boldsymbol{q}}_t(\tau)$ satisfies Eq. (3). Thus, the desired steering angle defined by Eq. (11) or Eq. (21) is well determined along the reference trajectory $\overline{\boldsymbol{q}}_t(\tau)$ (for $\overline{\boldsymbol{e}} = \boldsymbol{0}$) by the reference input $\boldsymbol{v}_t(\tau)$.

The time behavior of β_d in the case of a constant reference $\overline{\boldsymbol{q}}_t$ is generally more difficult to determine, since now $\boldsymbol{\phi}(\cdot) \to \boldsymbol{0}$ when $\overline{\boldsymbol{e}}(\tau)$ tends to zero. Thus terminally, definitions (11) and (21) are not well defined. Since $\overline{\boldsymbol{e}}(\tau) \to \boldsymbol{0}$ as $\tau \to \infty$,

[4] Lipschitz continuous in e_d for $\delta = 1$.

one can write: $\lim_{\tau\to\infty}\boldsymbol{\phi}(\overline{\boldsymbol{e}}(\tau),\tau)=\mathbf{0}$. Using additional definitions (22) and (23), one can analyze the limit $\beta_d^{\lim}=\lim_{\tau\to\infty}\beta_d(\boldsymbol{\phi}(\overline{\boldsymbol{e}}(\tau),\tau))$ to obtain the terminal behavior of steering variable β. Recalling again Eqs. (11) and (21), it is clear that terminal value of β_d depends on the convergence-rate ratio of $\phi_1(\cdot)$ and $\phi_2(\cdot)$. Generally, this ratio comes from structural properties of a particular stabilizing control function $\boldsymbol{\phi}(\cdot)$ selected by the user. Therefore, it is possible to claim about $\beta_d^{\lim}$ only assuming a special case of a selected stabilizer. Taking, for example, a properly tuned unicycle controller proposed in ref. [19], it can be shown that terminally $\phi_1(\cdot)$ always tends to zero faster than $\phi_2(\cdot)$, thus in this case $\beta_d^{\lim}=j\pi,\ j=0,1,2\ldots$. However, in general, if for a selected unicycle controller the convergence-rate ratio of $\phi_1(\cdot)$ and $\phi_2(\cdot)$ cannot be determined, the terminal value $\beta_d^{\lim}$ may not exist leading to permanent oscillations of $\beta_d(\tau)$ as $\tau\to\infty$.

Finally, we have to comment how the discontinuity related to the condition $\|\boldsymbol{\phi}(\cdot)\|=0$ influences stability of the closed-loop system during a transient stage. Note that for a time-varying reference $\overline{\boldsymbol{q}}_t(\tau)$ and for a constant $\overline{\boldsymbol{q}}_t$, condition $\|\boldsymbol{\phi}(\cdot)\|=0$ implies $u_2(\|\boldsymbol{\phi}(\cdot)\|=0)=0$ (see Eqs. (9) and (19)). Therefore, the body-posture subsystem (7) does not move for $\|\boldsymbol{\phi}(\overline{\tau})\|=0$ (see Eqs. (8) and (18)) and the finite-time escape effect is not possible here. For the tracking case, only a slight temporary increase of the tracking error may hold (caused by the moving reference point $\overline{\boldsymbol{q}}_t(\tau)$), which, however, can be again attenuated for $\tau>\overline{\tau}$ (condition $\|\boldsymbol{\phi}(\cdot)\|=0$ cannot be persistent by assumption). If one applies a more practical condition $\|\boldsymbol{\phi}(\cdot)\|<\varepsilon$ for $\varepsilon>0$ together with the switching $u_2(\|\boldsymbol{\phi}(\cdot)\|<\varepsilon)=:0$ (see Remark 2) for activation of additional definitions (22) and (23) or (24), then the temporary increase of the tracking error may be a little higher since the vehicle posture stays in ε for some finite time interval. In the case of set-point regulation, application of the practical condition with switching $u_2(\|\boldsymbol{\phi}(\cdot)\|<\varepsilon):=0$ implies that the vehicle posture stops at some vicinity $\varepsilon^*=\varepsilon^*(\varepsilon,\cdot)>0$ of the reference point and stays there if $\|\boldsymbol{\phi}(\cdot)\|$ is nonincreasing for future time: $\forall\tau>\tau^*\ \|\overline{\boldsymbol{e}}(\tau)\|=\varepsilon^*(\varepsilon,\cdot),\ \tau^*:\ \|\boldsymbol{\phi}(\tau^*)\|=\varepsilon$. In this case, one obtains only the ultimate boundedness (see ref. [10]) of the error $\overline{\boldsymbol{e}}$ rather than its asymptotic convergence to zero.

It is worth to note that for $e_d=0$ (hence, for $\beta=\beta_d$) the inputs defined by Eqs. (8) and (18) of the body-posture subsystem (7) are equal to the nominal unicycle control functions: $v_1=\phi_1,\ v_2=\phi_2$. This can be easily shown by substituting definitions (9) and (19) with $\beta=\beta_d$ into Eqs. (8) and (18), respectively, and using relation (10) or (20).

4. Simulation Examples

To illustrate the effectiveness of the proposed control strategy, six simulation examples E1–E6 are discussed using different unicycle controllers presented in the literature. To obtain simplicity and variety of exposition, a set of widely known and well established as well as novel unicycle controllers has been selected. The first two examples present the control quality for the trajectory tracking task using linearization-based[6] and Vector-Field-Orientation (VFO)[19] unicycle controllers. The third example, slightly different in nature compared to tracking but practically important, illustrates the path-following task utilizing the Samson's nonlinear controller.[27] The last three simulations illustrate performance obtained in the set-point regulation task with the smooth time varying[25] and two discontinuous time-invariant stabilizers.[15,19] All simulations were run within the time horizon of $\tau_h=20$ s using the kinematic model (1) or (2) with the geometric parameter $L=0.2$ m and with the steering controller gain $k_d=10$ (compare Eq. (14)). The basic conditions for the particular examples together with the values of selected parameters are summarized in Table I. The plots of the paths and the robot configurations on the plane are denoted as follows: reference trajectory—solid black line, path drawn by the robot—dashed gray line, robot configurations—green skeletons, initial robot configuration—red skeleton (a small circle denotes the *guidance point* of the vehicle platform and a star mark denotes the front part of the steered wheel). Further details of the conducted simulation tests are specified in the next subsections.

Table I. Selected parameters and conditions for simulation examples.

Ex.	Model	β_m	δ	Motion task	Unicycle controller
E1	FD	∞	1	Tracking	Linearization-based[6]
E2	RD	$\pi/3$	1	Tracking	VFO[19]
E3	FD	$\pi/2$	1	Path following	Nonlinear[27]
E4	RD	$\pi/3$	2/3	Regulation	Time varying[25]
E5	RD	$\pi/4$	1	Regulation	Time invariant[15]
E6	FD	$\pi/2$	1	Regulation	VFO[19]

4.1. Tracking with the linearization-based controller (E1)

The first unicycle tracking controller selected in example E1 was taken from ref. [6]. Its structure results from linearization of the closed-loop error dynamics along a reference trajectory $\overline{\boldsymbol{q}}_t(\tau)$. The nominal unicycle control functions are represented as follows:

$$\phi_1=\phi_{1t}+k_3(\boldsymbol{\phi}_t)\mathrm{sgn}(\phi_{2t})e_3-k_1(\boldsymbol{\phi}_t)e_1, \tag{43}$$

$$\phi_2=\phi_{2t}\cos e_1+k_2(\boldsymbol{\phi}_t)e_2, \tag{44}$$

where $k_1(\boldsymbol{v}_t)=k_2(\boldsymbol{v}_t)=2\xi\sqrt{v_{1t}^2+bv_{2t}^2}$, $k_3(\boldsymbol{v}_t)=b\,|v_{2t}|$, $\xi,b>0$, and $\boldsymbol{e}=[e_1\,e_2\,e_3]^{\mathrm{T}}=\boldsymbol{R}_z(-\theta)\overline{\boldsymbol{e}}$ with $\boldsymbol{R}_z(\cdot)\in SO(3)$ being the basic rotation operator around z-axis. The reference signals, particular values, and initial conditions were selected as follows: $v_{1t}(\tau)=-0.3+0.5\sin(2\tau)$, $v_{2t}(\tau)=0.2+0.05\sin(2\tau)$ (forward reference motion), $\overline{\boldsymbol{q}}_t(0)=\mathbf{0}$, $\boldsymbol{q}(0)=[0\ \ 0\ \ -0.2\ \ -0.4]^{\mathrm{T}}$, $\xi=1$, $b=10$. Simulations were run for FD motorization with $\beta_m=\infty$ using steering controller (14) with $\delta=1$. The results are presented in Fig. 3.

4.2. Tracking with the VFO controller (E2)

The second unicycle tracking controller was chosen to be the VFO controller proposed in ref. [19]. The VFO control structure results from simple geometrical interpretations related to the unicycle kinematics, from introduction of the so-called *convergence vector field*, and from decomposition of the control process into the *orienting* and *pushing*

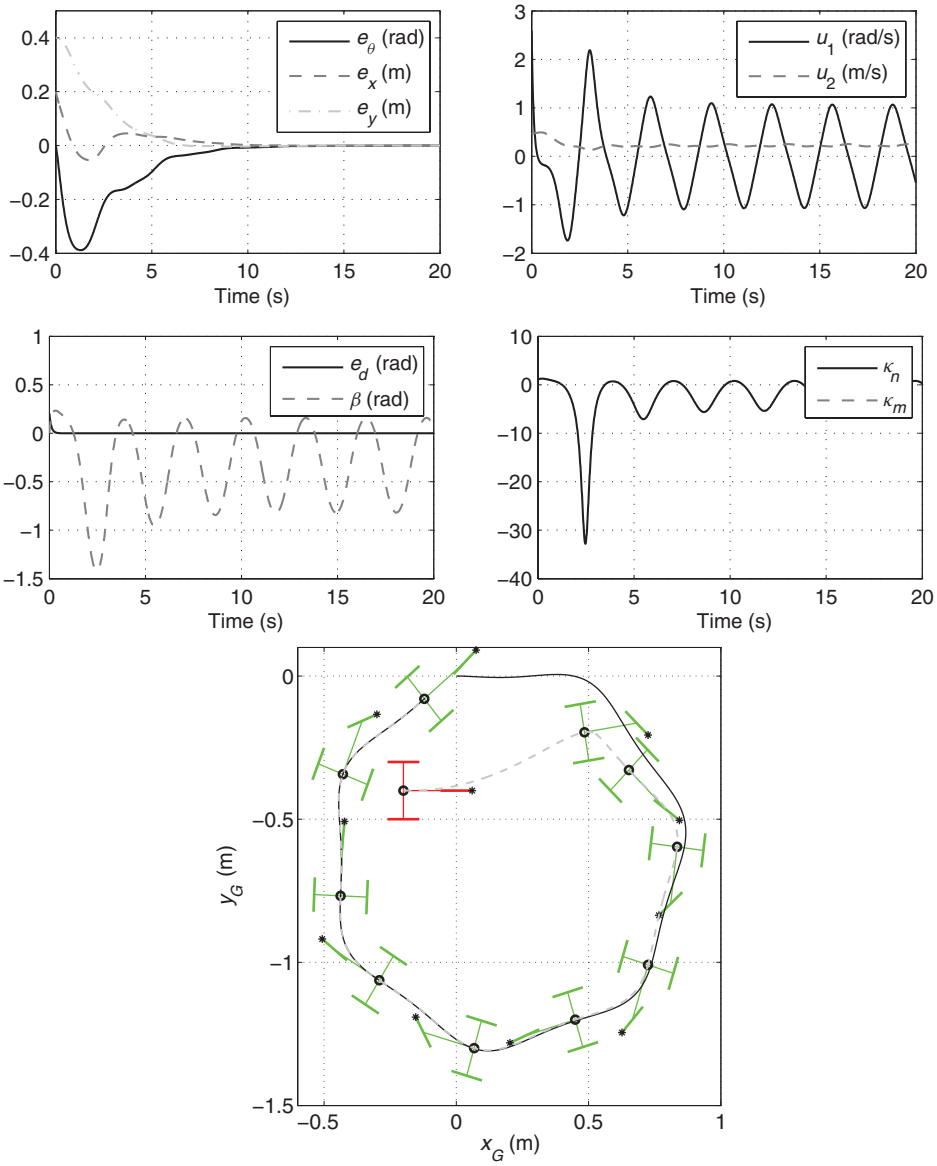

Fig. 3. (Colour online) E1: Simulation results of the trajectory tracking task with an FD car-like robot using the linearization-based unicycle controller (initial robot configuration has been highlighted in red).

subprocesses. The nominal unicycle VFO control inputs are defined as follows:

$$\phi_1 = k_a(\theta_a - \theta) + \dot{\theta}_a, \tag{45}$$

$$\phi_2 = h_x \cos\theta + h_y \sin\theta, \tag{46}$$

where $\theta_a = \text{Atan2c}(\sigma h_y, \sigma h_x)$, $\sigma = \text{sgn}(v_{2t}(\tau))$, $\dot{\theta}_a = (\dot{h}_y h_x - h_y \dot{h}_x)/(h_x^2 + h_y^2)$, and $\boldsymbol{h}^* = [h_x \; h_y]^{\mathrm{T}} = k_p \boldsymbol{e}^* + \dot{\boldsymbol{q}}_t^*$, $\boldsymbol{e}^* = [e_x \;\; e_y]^{\mathrm{T}}$, $\dot{\boldsymbol{q}}_t^* = [\dot{x}_t \;\; \dot{y}_t]^{\mathrm{T}}$. The constants $k_a, k_p > 0$ are the design parameters. Simulations were run for RD motorization with $\beta_m = \pi/3$ using steering controller (14) with $\delta = 1$, and selecting: $v_{1t}(\tau) = -0.3 + 0.5\sin(2\tau)$, $v_{2t} = -0.2 + 0.05\sin(2\tau)$ (backward reference motion), $\overline{\boldsymbol{q}}_t(0) = \boldsymbol{0}$, $\boldsymbol{q}(0) = [0\,0\;\; -0.2\,0.5]^{\mathrm{T}}$, and $k_a = 5, k_p = 2$. The results obtained are presented in Fig. 4.

4.3. Path following with the nonlinear controller (E3)

For a path-following task, we have used the nonlinear unicycle controller proposed by Samson in ref. [27]. The nominal unicycle control functions are defined as

$$\phi_1 = -k_2 V \frac{\sin e_\theta}{e_\theta} D - k_3 |V| e_\theta + \frac{V \kappa_p \cos e_\theta}{1 - D\kappa_p}, \tag{47}$$

$$\phi_2 = V, \tag{48}$$

where $k_{2,3} > 0$ are design parameters, $V \neq 0$ is an assumed and constant driving velocity of the vehicle, κ_p is a current curvature of the path, and $e_\theta = \theta - \theta_d$ is an orientation error along the path with θ_d being the desired orientation on the path. For simulations, the circular desired path of radius R and centered at the origin was selected. The position error $D = R - \sqrt{x^2 + y^2}$ denotes the shortest distance to the path. The following values and definitions were used: $\boldsymbol{q}(0) = [0 \;\; 0 \;\; -0.2 \;\; 0.5]^{\mathrm{T}}$, $R = 1/\kappa_p = 0.7$ m, $V = 0.3$ m/s, $k_2 = 16, k_3 = 8, \theta_d = \text{Atan2c}(y, x) + \pi/2$. Simulations were run for FD motorization with $\beta_m = \pi/2$ using steering controller (14) with $\delta = 1$. The results are presented in Fig. 5.

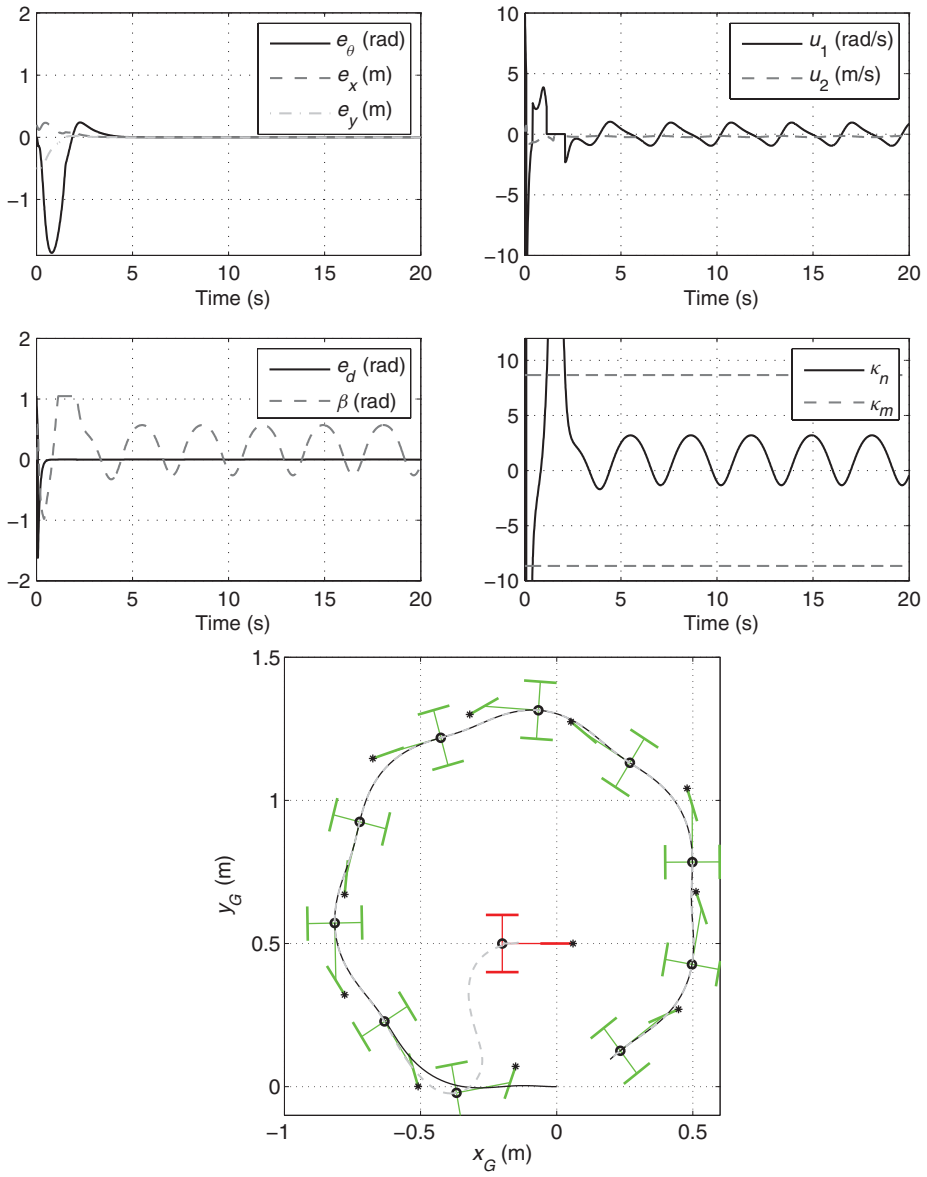

Fig. 4. (Colour online) E2: Simulation results of the trajectory tracking task with an RD car-like robot using the VFO unicycle controller (initial robot configuration has been highlighted in red).

4.4. Set-point regulation with time-varying controller (E4)

Example E4 concerns a set-point regulation task with the smooth time-varying stabilizer obtained by using the general design method proposed by Pomet in ref. [25]. By defining the Lyapunov function $V = \frac{1}{2}k_1(e_1 + h)^2 + \frac{1}{2}(k_2e_2^2 + k_3e_3^2)$ for the error dynamics with $k_{1,2,3} > 0$, where $h = h(\boldsymbol{e}, \tau) = k_4 \left\| \boldsymbol{e}^* \right\| \cos(\omega\tau)$ is a time-varying component with $\omega, k_4 > 0$, and $\boldsymbol{e} = [e_1\ e_2\ e_3]^{\mathrm{T}} = -\boldsymbol{R}_z(-\theta_t)\overline{\boldsymbol{e}}$ with $\boldsymbol{R}_z(\cdot) \in SO(3)$, the following unicycle control functions are obtained:

$$\phi_1 = \omega k_4 \left\| \boldsymbol{e}^* \right\| \sin(\omega\tau) - k_1(e_1 + h), \tag{49}$$

$$\phi_2 = -k_2e_2 - k_3e_3 - 4k_1k_4 \left\| \boldsymbol{e}^* \right\| (e_1 + h)\cos(\omega\tau), \tag{50}$$

with $\boldsymbol{e}^* = [e_2\ e_3]^{\mathrm{T}}$. For simulation purposes, the reference point, initial conditions, and the parameter values were selected as $\overline{\boldsymbol{q}}_t = \boldsymbol{0}$, $\boldsymbol{q}(0) = [0\ 0\ 0.5\ 0.5]^{\mathrm{T}}$, $k_{1,2,3} = 2$, and $\omega = k_4 = 1$. In this case, the finite-time steering controller (14) was used with $\delta = 2/3$. Simulations were run for RD motorization with $\beta_m = \pi/3$. The results are presented in Fig. 6.

4.5. Set-point regulation with time-invariant controllers (E5, E6)

In the example E5, we applied the discontinuous time-invariant controller considered by Kim and Tsiotras in ref. [15] to solve a set-point regulation task. The unicycle control functions obtained for the chained-form transformation of the original kinematics are as follows:

$$\phi_1 = -kx_2 - \mu x_1\big(x_3 - 0.5x_1x_2\big)/\big(x_1^2 + x_2^2\big), \tag{51}$$

$$\phi_2 = -kx_1 + \mu x_2\big(x_3 - 0.5x_1x_2\big)/\big(x_1^2 + x_2^2\big), \tag{52}$$

where $k, \mu > 0$ are design parameters, $x_1 = e_2\cos e_1 + e_3 \sin e_1$, $x_2 = e_1$, $x_3 = e_2 \sin e_1 - e_3 \cos e_1$ are the definitions of the chained-form system states in the error space, and $\boldsymbol{e} = [e_1\ \ e_2\ \ e_3]^{\mathrm{T}} = -\boldsymbol{R}_z(-\theta_t)\overline{\boldsymbol{e}}$ with $\boldsymbol{R}_z(\cdot) \in SO(3)$.

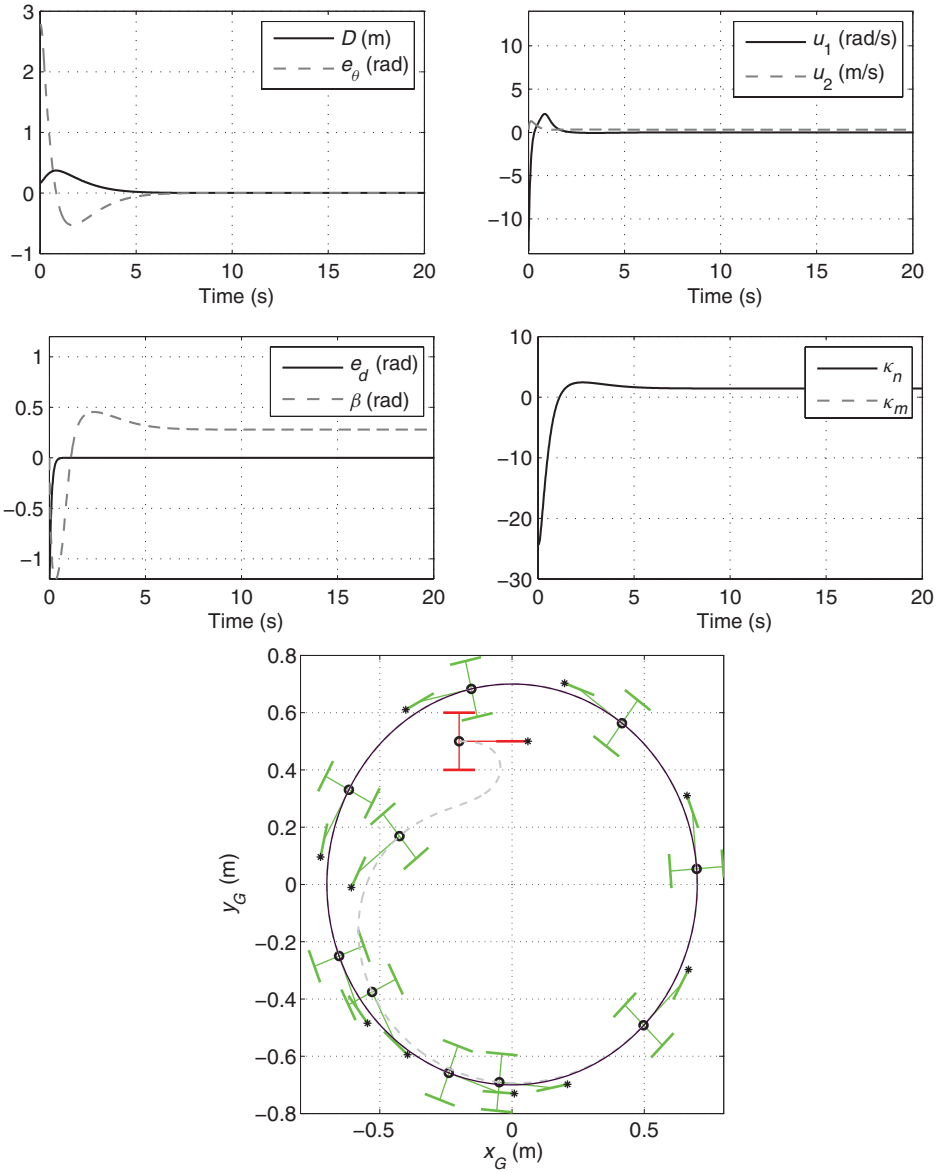

Fig. 5. (Colour online) E3: Simulation results of the path-following task with an FD car-like robot using Samson's nonlinear unicycle controller (initial robot configuration has been highlighted in red).

Simulations were run for RD motorization with $\beta_m = \pi/4$ using steering controller (14) with $\delta = 1$ and taking $\overline{\boldsymbol{q}}_t = \mathbf{0}$, $\boldsymbol{q}_0 = [0\ 0\ 0.5\ 0.5]^{\mathrm{T}}$, $k = 0.5$, and $\mu = 2$. The results are presented in Fig. 7.

The last examined controller (example E6) was the VFO stabilizer presented in ref. [19]. Origins of the VFO stabilizer are the same as for the tracking controller recalled in example E2. The unicycle control functions for the controller are the same as in Eqs. (45) and (46), but now $\sigma = \{-1, +1\}$ is a decision factor, and $\boldsymbol{h}^* = [h_x\ \ h_y]^{\mathrm{T}} = k_p \boldsymbol{e}^* + \boldsymbol{v}^*$, $\boldsymbol{v}^* = -\eta\, \sigma \parallel \boldsymbol{e}^* \parallel \boldsymbol{g}^*_{2t}$, $\boldsymbol{g}^*_{2t} = [\cos\theta_t\ \ \sin\theta_t]^{\mathrm{T}}$. The constant $\eta \in (0, k_p)$ is an additional design parameter (in comparison to the VFO tracking controller). Simulations were run for FD motorization with $\beta_m = \pi/2$ using steering controller (14) with $\delta = 1$, and selecting $\sigma = -1$ (backward parking maneuvers), $\overline{\boldsymbol{q}}_t = \mathbf{0}$, $\boldsymbol{q}(0) = [0\ 0\ 0.1\ 0.8]^{\mathrm{T}}$, and $\eta = 1.5$ (other parameters were the same as for the VFO tracking case). The obtained results are presented in Fig. 8. It is worth noting that the two control laws examined in this subsection are not Lyapunov stable, since the origin is not an equilibrium of a closed-loop system—in this case, we can talk about *almost stabilizers*.[15]

4.6. *Comments to the results*

The time plots of body-posture errors in Figs. 3 and 4 show asymptotic and relatively fast convergence toward zero, especially for the VFO unicycle controller. In example E1, the maximal admissible curvature is infinite, thus the whole plot of κ_n (nominal curvature determined by the unicycle controller) stays within the admissibility bounds. However, in example E2, the feasible curvature is substantially limited, and for some initial time intervals κ_n violates the bounds (assumption A4 is temporarily not met). Despite these occasional violations, the vehicle motion is then successfully completed, what can justify relaxation of A4 for some time intervals as mentioned in Section 2. Note that in both examples E1 and E2, the oscillatory behavior of β variable results directly from the selected nonconstant reference input $v_{1t}(\tau)$, which

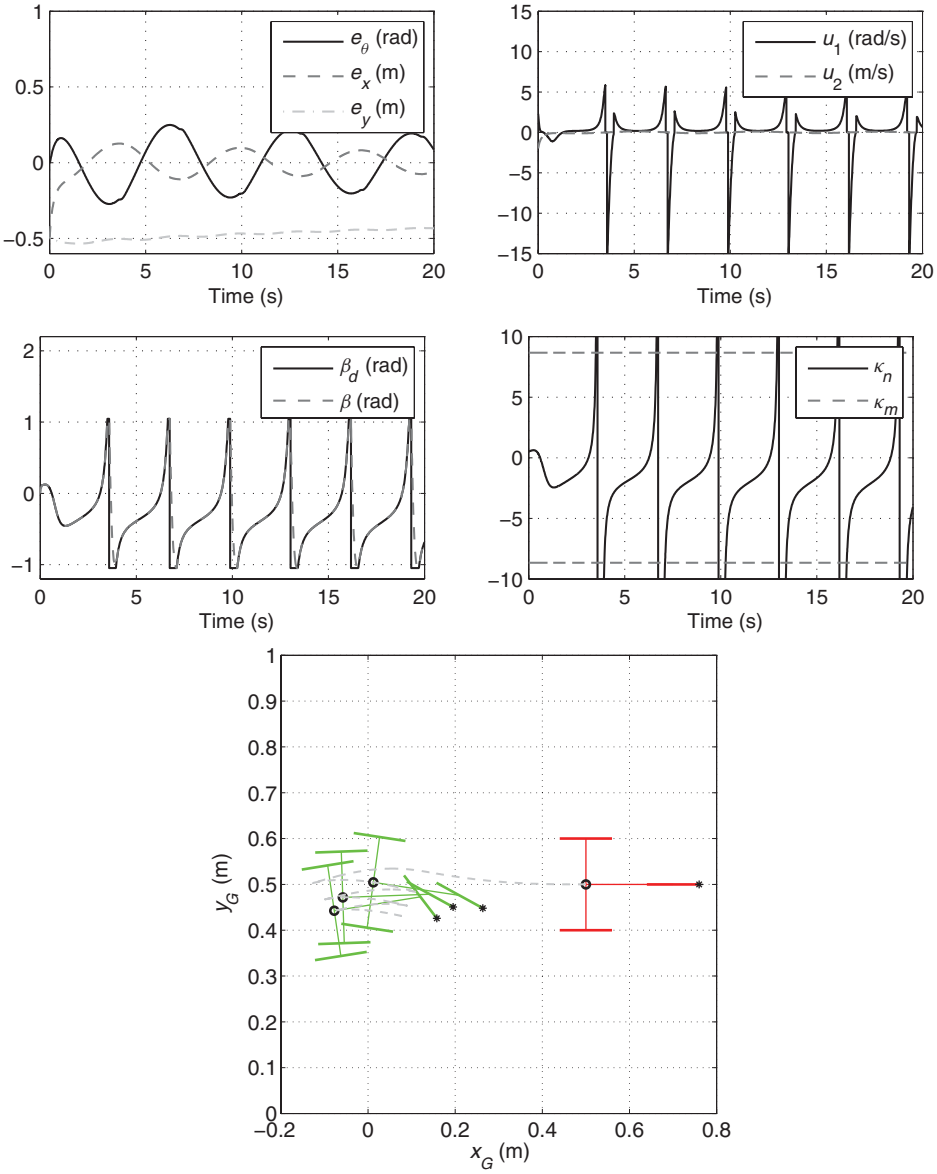

Fig. 6. (Colour online) E4: Simulation results of the set-point regulation task with an RD car-like robot using the smooth time-varying unicycle controller (initial robot configuration has been highlighted in red).

defines the time-varying angular velocity of the robot body. Since the car-like kinematics is a differentially flat system, the behavior of $\beta(\tau)$ for $\overline{\boldsymbol{e}} \approx \mathbf{0}$ is fully determined by time evolution of the flat outputs (x, y) and their time derivatives.

Note also good convergence for the path-following task as illustrated by Fig. 5. In this case—since the constant-curvature circular path was chosen—the steering angle β converges to the constant value and does not oscillate.

Control quality for the most demanding set-point regulation task has been presented in examples E4–E6 using two stabilizers characterized by oscillatory behavior, and one stabilizer leading to nonoscillatory transients. Frequent oscillations obtained in examples E4 and E5 are related to frequent robot-body motion reversals, and consequently, frequent passing through zero for $\phi_2(\cdot)$. Recalling definition (21), it is evident that this effect can imply more intensive violations of the steering bound β_m as can be seen from Figs. 6 and 7. But again, if the number of violation time-instants is not dense, the effective stabilization is still possible driving the robot body to the reference point. As predicted in the theoretical analysis from Section 3.1, for the examined oscillatory stabilizers, the limit for $\beta_d(\tau)$ does not exists, and the steering wheel is persistently reorienting (compare Figs. 6 and 7). Much slower body-posture error convergence obtained for E4 in comparison with E5 is a direct consequence of the well-known features of smooth time-varying stabilizers. Different behavior can be seen in example E6, where the VFO stabilizer was used. Due to the characteristic geometrical features of the VFO control strategy,[19] the first nominal input $\phi_1(\tau)$ terminally always tends to zero faster than $\phi_2(\tau)$ as $\tau \to \infty$. This directly implies the final convergence of $\beta_d(\tau)$ to its limit zero value for $\tau \to \infty$ as can be seen in Fig. 8.

4.7. *Limitations of the method—negative examples*

Examples E1–E6 illustrate the effectiveness of the proposed control scheme under assumptions A1–A4. It may be interesting to check how violation of the assumptions

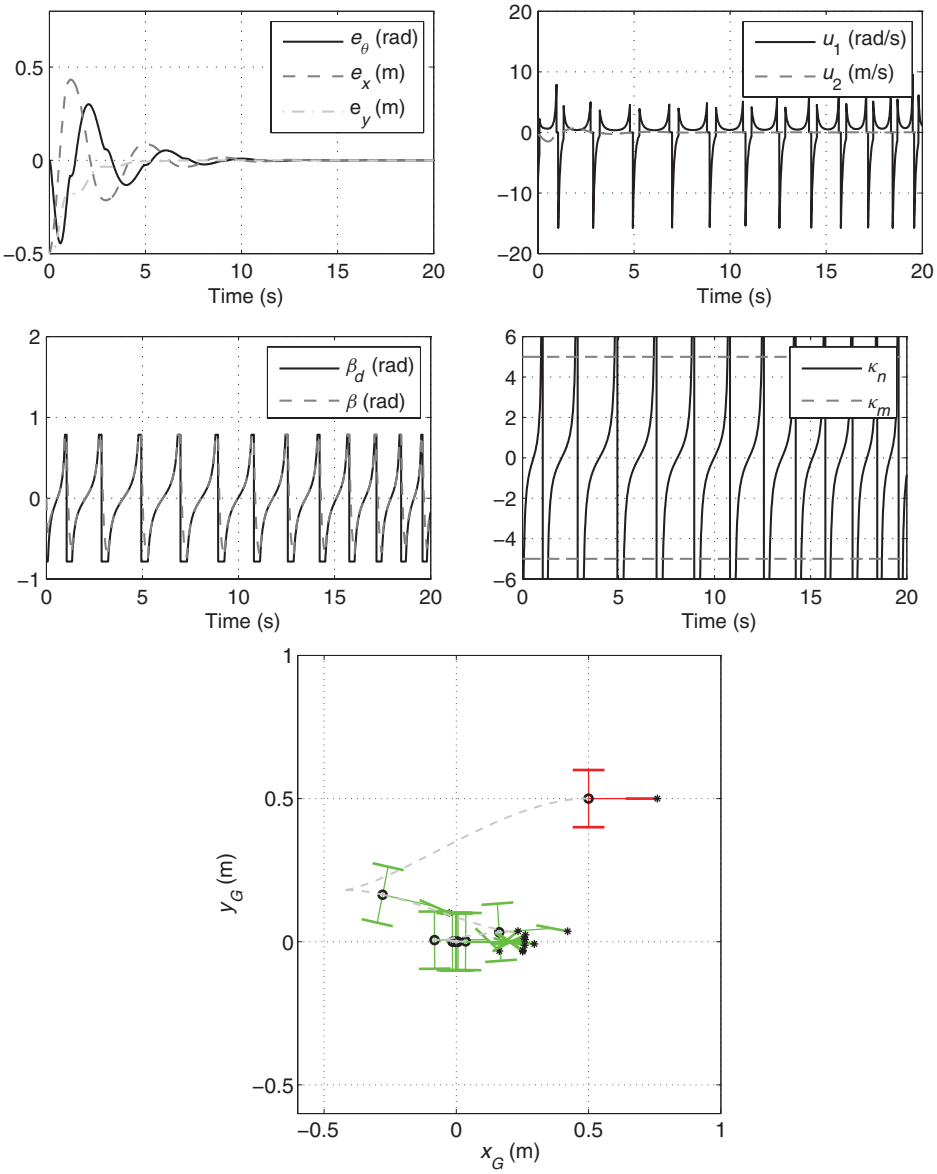

Fig. 7. (Colour online) E5: Simulation results of the set-point regulation task with an RD car-like robot using the discontinuous time-invariant unicycle controller (initial robot configuration has been highlighted in red).

influences behavior of the closed-loop system. Let us take into account assumptions A2 and A4, since they are directly related to the limitations on the steering angle β that are often imposed in applications. In the sequel, two negative examples are presented: NE1, where the feasibility condition A4 cannot be met, and NE2, where the reference trajectory violates the maximal-curvature condition A2.

Violation of A4 within a dense time interval can lead to the lack of body-posture convergence—the vehicle gets stuck in some configuration point away from the reference one. Figure 9 presents such an exemplary situation obtained for the time-invariant VFO controller and the parameters selected as, for example, E6 but with $\beta_m = \pi/4$. Demand of the high motion curvature during a final stage of parking maneuvers causes in this case too intensive violation of condition A4. It is indicated by the plot of the nominal motion curvature $\kappa_n(\tau)$, which permanently violates the vehicle curvature bounds after about 2.5 s of the simulation. As illustrated by the plots of the posture error norm $\|\overline{e}(\tau)\|$ (denoted "Ne" in the figure) and the control inputs $u_1(\tau), u_2(\tau)$, it can be seen that the closed-loop system remains stable with bounded controls but the vehicle gets stuck in the neighborhood of the reference point[5]. One can try to cope with this situation by proper introduction (on a motion planning stage) of a via-point between the initial posture and the reference one assuring sufficient limitation of the nominal motion curvature.

Figure 10 illustrates control quality deterioration resulting from violation of assumption A2. The results were obtained using the linearization-based tracking controller assuming the same conditions as, for example, E1 but with $\beta_m = \pi/5$. In this case, the reference trajectory (generated for the unicycle model) periodically requires higher (in the sense of the absolute value) motion curvature than the car-like vehicle is able to achieve. It is visible on the plot of the nominal motion curvature $\kappa_n(\tau)$ that periodically crosses

[5] It is worth to note that the considered maneuvers were successfully completed using $\beta_m = \pi/3$.

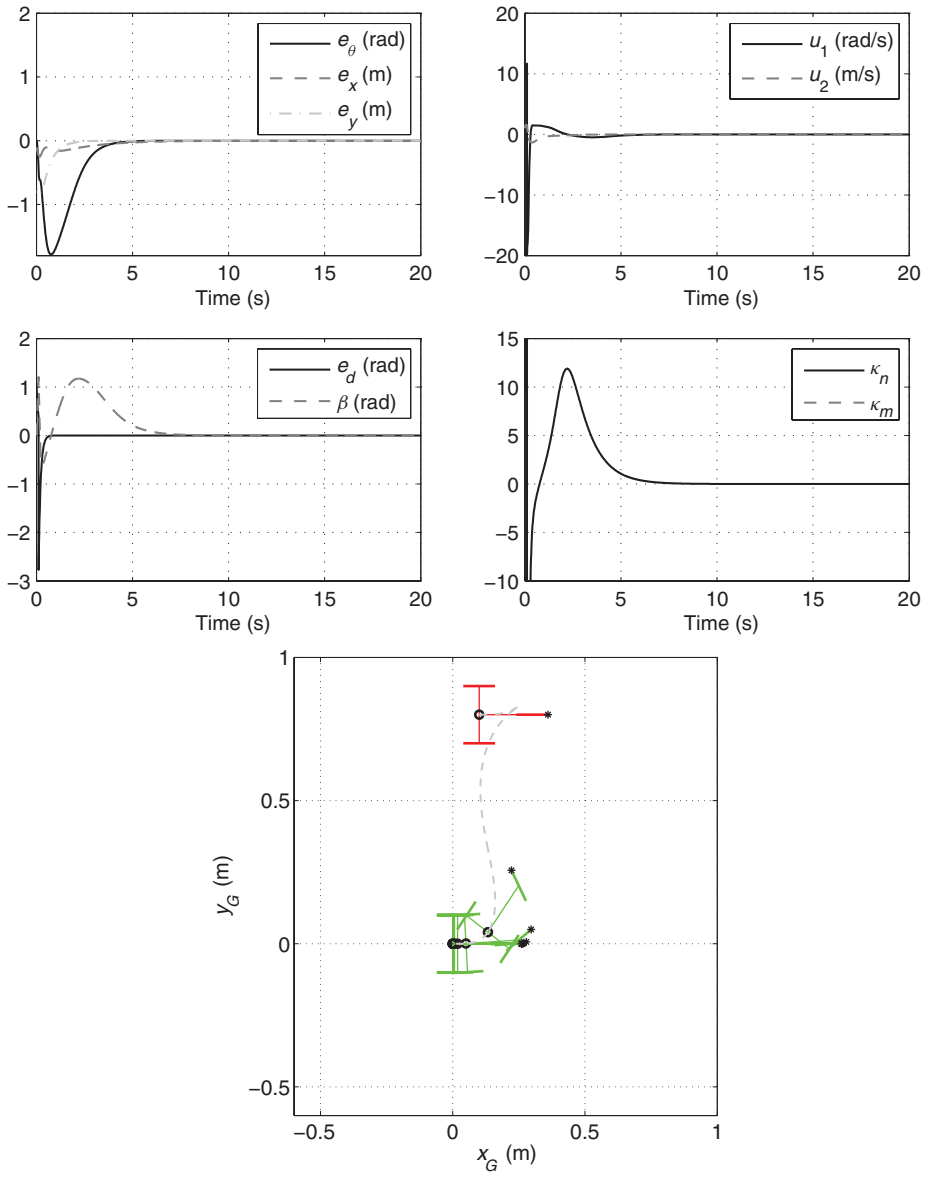

Fig. 8. (Colour online) E6: Simulation results of the set-point regulation task with an RD car-like robot using the VFO time-invariant unicycle controller (initial robot configuration has been highlighted in red).

the curvature bounds after about 5 s of the simulation. The plot of the posture error norm $\|\overline{\boldsymbol{e}}(\tau)\|$ (denoted "Ne" in the figure) reveals that the asymptotic convergence was lost in this case; however, the stability of the closed-loop system was preserved leading to the ultimate boundedness of the errors. Since the curvature bound of the car-like robot is only slightly less than this required by the reference trajectory, the resulting motion quality of the vehicle seems to be acceptable in some less demanding applications. Further deterioration in the tracking precision is presented on the X–Y plot on the right-hand side in Fig. 10, where the maximal steering angle was limited to $\beta_m = \pi/8$.

4.8. *Practical implementation issues*

In practical implementation of the proposed control framework, three main issues are worth attention. The first one is the robustness of the method to the model parametric uncertainty, which in case of kinematics (1) and (2) is related to a value of parameter L that in practice is unknown exactly. The second problem concerns noisy measurements of feedback signals and their influence on the closed-loop system stability and performance. The third issue is related to the problem of satisfying the physical limitations imposed on the vehicle control inputs, which are always present in practical applications.

To verify control performance for the proposed method under all the practical conditions mentioned above, two additional exemplary simulations EP1 and EP2 were run. In order to examine robustness of the control system, an overestimated value of the vehicle parameter $L_s = 1.1\,\mathrm{L}$ was introduced into the controller equations. Furthermore, the zero-mean Gaussian measurement noises were added to the feedback loop with the following standard deviations: $\sigma_\beta = 0.0001$, $\sigma_\theta = 0.0032$, $\sigma_x = \sigma_y = 0.001$, respectively. To cope with the control input limitations, the following on-line scaling procedure was applied (the similar procedure for

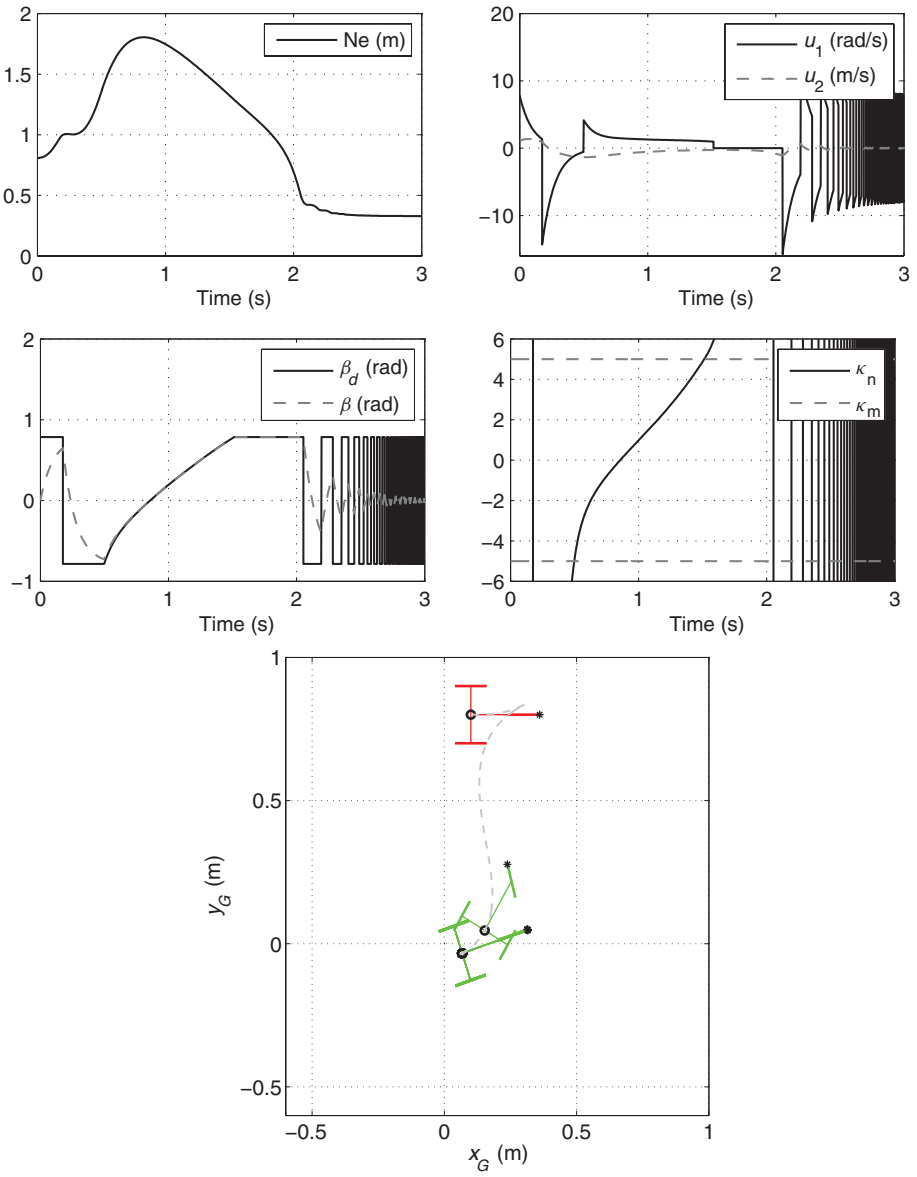

Fig. 9. (Colour online) NE1: Simulation results for the negative example of set-point regulation where the feasibility condition A4 is not met (the results for RD motorization with $\beta_m = \pi/4$); initial robot configuration has been highlighted in red.

the unicycle-like kinematics was used in ref. [19]):

$$\boldsymbol{u}_s = \frac{1}{s}\boldsymbol{u}, \quad s \triangleq \max\left\{1; \frac{|u_1|}{u_{1\max}}; \frac{|u_2|}{u_{2\max}}\right\} \in (0, 1], \quad (53)$$

where $\boldsymbol{u}_s$ denotes the scaled (physically feasible) control input vector that satisfies the imposed limits $u_{1\max} > 0$ and $u_{2\max} > 0$, while $\boldsymbol{u}$ in Eq. (53) is the *unlimited* control input computed according to the control law defined in Section 3. During simulations, the following limits were selected: $u_{1\max} = 3$ rad/s and $u_{2\max} = 0.3$ m/s for test EP1, and $u_{1\max} = 3$ rad/s and $u_{2\max} = 1$ m/s for test EP2. Simulation EP1 was run using the VFO tracking controller under the conditions defined in example E2 but with lower design gains $k_d = 4$, $k_p = 1$, and $k_a = 2$. Simulation EP2 was organized according to conditions defined in example E5. The results are shown in Figs. 11 and 12, where the plots in the upper row illustrate the results obtained without the measurement noises, and in the lower row—with the noises added to the feedback loop.

Analyzing the results, one can find acceptable robustness of the method to the model parametric uncertainty. In the case of set-point control, the asymptotic convergence was preserved. For the tracking case, one can expect only the ultimate boundedness of the tracking error. On the other hand, the feedback measurement noises are better tolerable in the case of permanent motion of the vehicle as can be seen in Fig. 11. For the set-point control when the posture errors become very small and amplitudes of the control functions ϕ_1 and ϕ_2 approach the noise level, the desired steering angle computed by Eq. (11) or Eq. (21) is mostly driven by the noise causing oscillatory character of the control input u_1, clearly visible in Fig. 12. Let us also stress here that the robustness of the whole closed-loop control system results not only from the proposed control framework but some properties are also inherited from the unicycle stabilizer selected in Eq. (4).

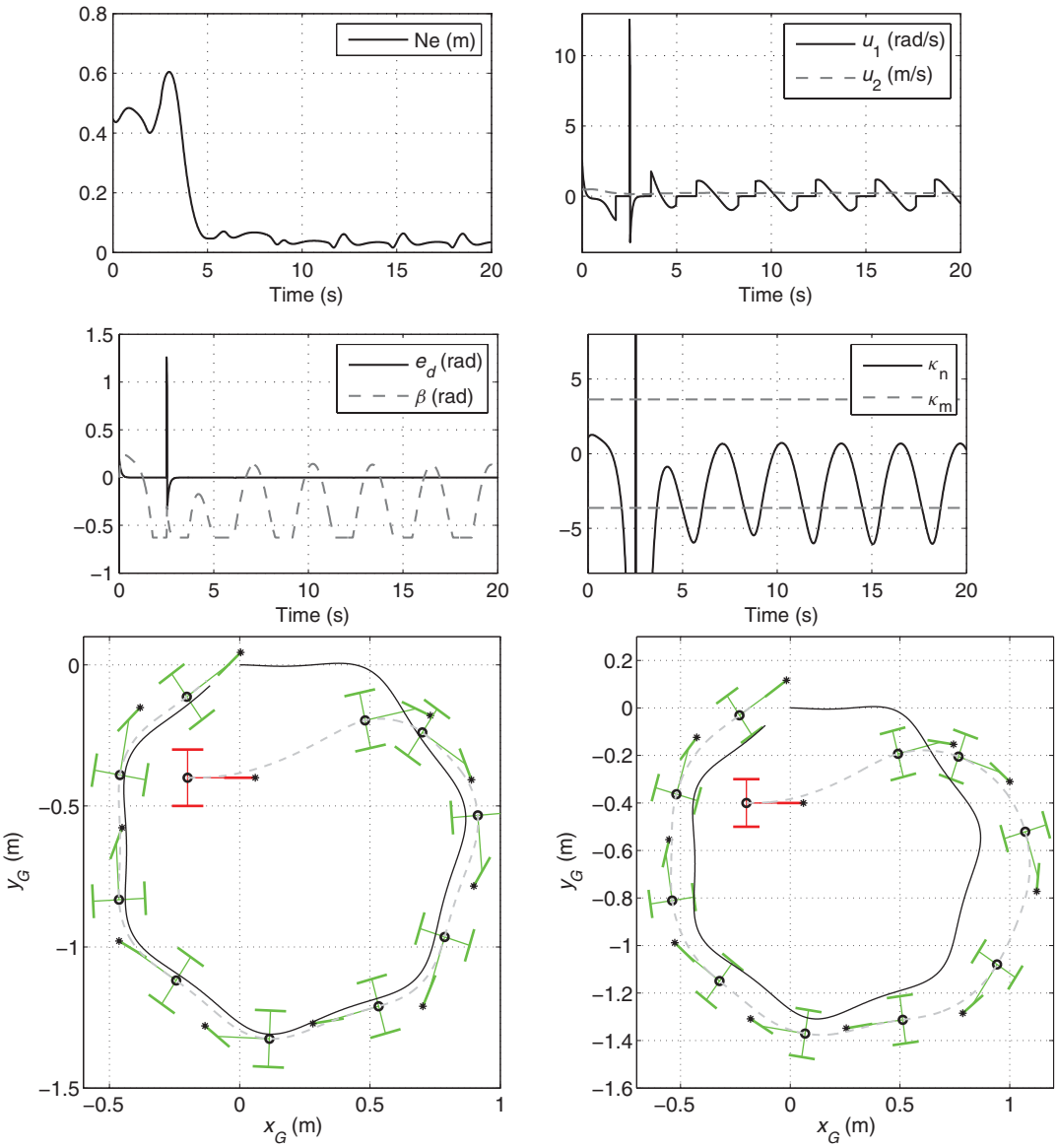

Fig. 10. (Colour online) NE2: Simulation results for the negative example of a tracking task where the reference trajectory periodically violates condition A2 (the results for FD motorization with $\beta_m = \pi/5$; the additional X–Y plot on the right-hand side illustrates motion performance for $\beta_m = \pi/8$); initial robot configuration has been highlighted in red.

From the time plots of control signals, one may conclude that the simple scaling procedure (53) is efficient preserving the control input limitations during the whole control time-horizon. Alternative solutions satisfying the state and input bounds have recently been proposed for instant in ref. [13] using the linear matrix inequalities (LMI) approach.

5. Concluding Remarks

In the paper, the general feedback control framework for the car-like robots has been proposed, which makes it possible to use the unicycle controllers with the more involved car-like kinematics. The method can be applied to both types of motorizations—with a FD and with a RD. All the possible ranges (limited and unlimited) of the steering wheel angle have been considered and examined. The concept proposed assumes that the vehicle-body subsystem plays a crucial role in a motion task, treating the steering wheel angle as an auxiliary configuration variable. This means that the steering angle is forced to follow its desired profile, computed in a way that guarantees error convergence for the vehicle body. Therefore, any convergence of the steering variable has to be treated as a side effect of the strategy formulated above together with intrinsic features of the utilized unicycle controller. According to the results presented the steering angle converges properly in the case of trajectory tracking and path-following tasks due to the differential flatness of the car-like kinematics. Lack of convergence for the desired steering angle occurs for the examined oscillatory set-point stabilizers, but it seems not to be very limiting in many practical applications. Stabilizers with characteristic features leading to faster terminal convergence for one of the unicycle control functions can lead to the existence of a desired steering angle limit, consequently guaranteeing convergence also for the steering configuration variable. Since the characteristics of the unicycle controllers are inherited by the proposed control method (in the sense of

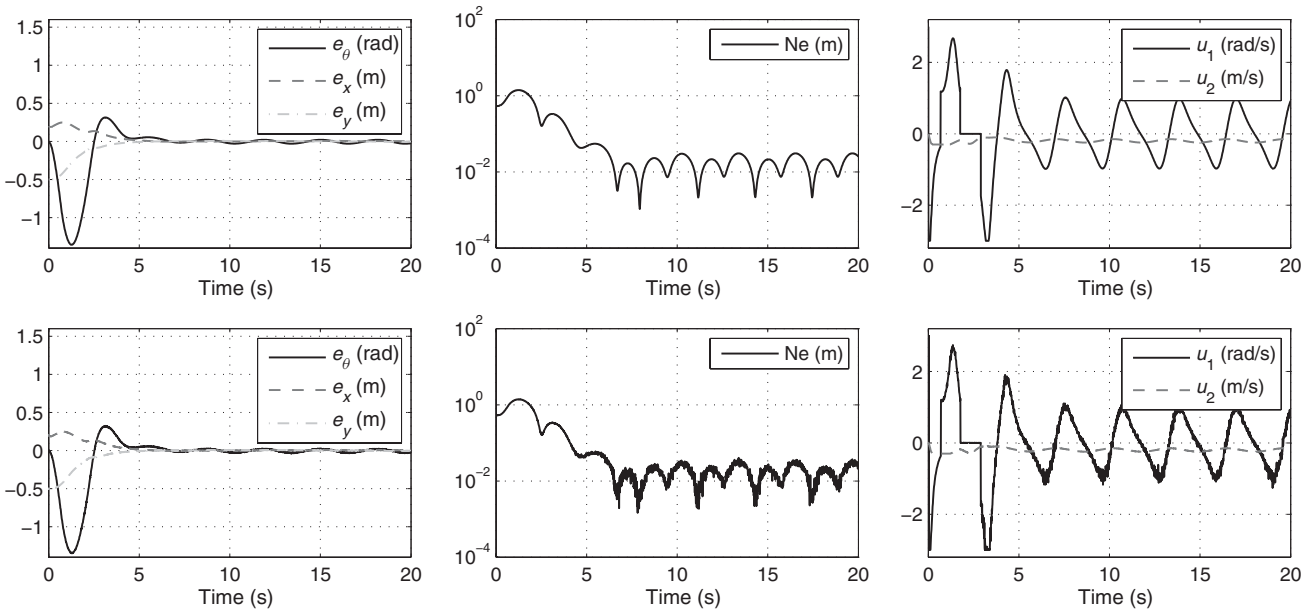

Fig. 11. EP1: Simulation results of the trajectory tracking task tested under practical conditions. In the middle column, the time evolution of $\|\bar{\boldsymbol{e}}\|$ is shown in the logarithmic scale.

the robot-body motion), successful practical utilization of the unicycle controllers in the proposed scheme depends on satisfaction of the *motion-curvature feasibility assumption* A4 related to the maximal motion curvature required during control task realization. Summarizing, the control method proposed in the paper can be treated as a simplified and complementary solution in comparison to the existing control laws dedicated to the car-like kinematics. Its usage may be effective especially in those practical motion control tasks where the terminal convergence of the vehicle steering subsystem is not critical.

Appendix. Derivation of the body-posture input v in the form of Eq. (35)

For compactness, the following notation will be used hereafter: $sa \equiv \sin a$, $ca \equiv \cos a$. In the computations below $\boldsymbol{v} = [v_1\ v_2]^{\mathrm{T}}$ denotes the control input vector of the unicycle model introduced in Eq. (3) and then used in Eq. (7), and by $\boldsymbol{\phi} = [\phi_1\ \phi_2]^{\mathrm{T}}$ one denotes the unicycle control functions introduced in Eq. (4); the arguments of the functions are omitted for compactness.

Substituting, respectively, definition (9) into Eq. (8) for FD kinematics or Eq. (19) into Eq. (18) for the RD model leads

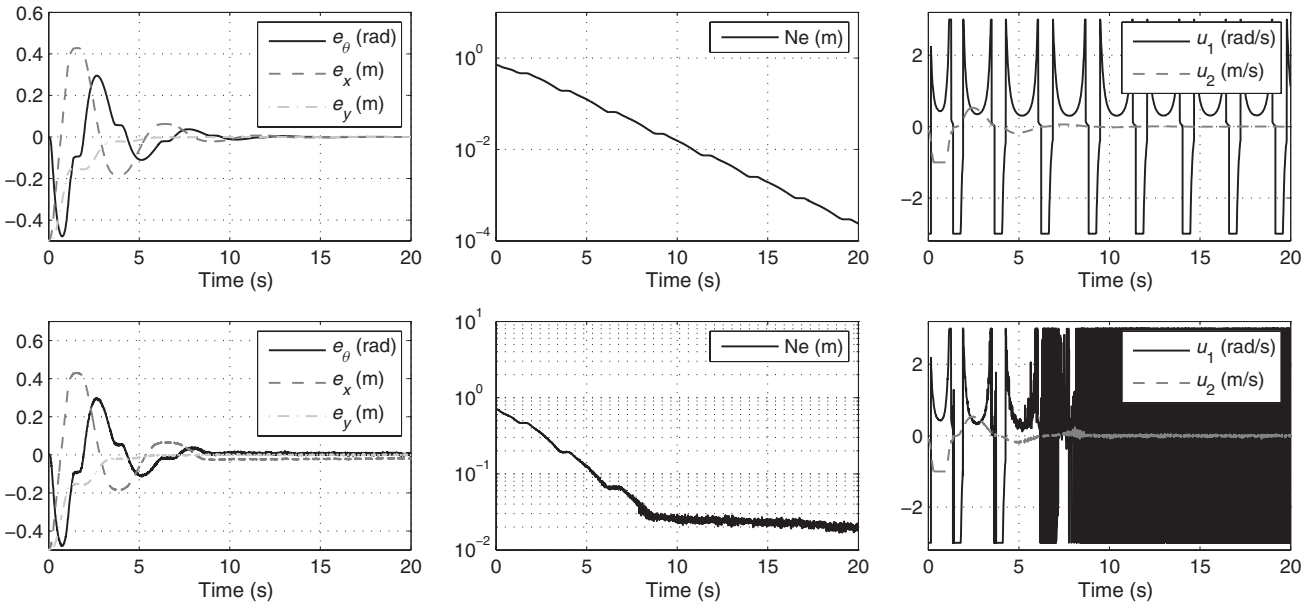

Fig. 12. EP2: Simulation results of the set-point regulation task tested under practical conditions. In the middle column, the time evolution of $\|\bar{\boldsymbol{e}}\|$ is shown in the logarithmic scale.

to

$$\begin{bmatrix} v_1 \\ v_2 \end{bmatrix} = \begin{bmatrix} \phi_1 \mathrm{s}^2\beta + \phi_2 \frac{1}{L}\mathrm{s}\beta\mathrm{c}\beta \\ \phi_1 L\mathrm{s}\beta\mathrm{c}\beta + \phi_2 \mathrm{c}^2\beta \end{bmatrix} = \begin{bmatrix} \mathrm{s}^2\beta + \frac{1}{L}\mathrm{s}\beta\mathrm{c}\beta \\ L\mathrm{s}\beta\mathrm{c}\beta + \mathrm{c}^2\beta \end{bmatrix} \begin{bmatrix} \phi_1 \\ \phi_2 \end{bmatrix}$$

$$= \left(\begin{bmatrix} 1 & 0 \\ 0 & 1 \end{bmatrix} + \begin{bmatrix} -\mathrm{c}^2\beta & \frac{1}{L}\mathrm{s}\beta\mathrm{c}\beta \\ L\mathrm{s}\beta\mathrm{c}\beta & -\mathrm{s}^2\beta \end{bmatrix} \right) \begin{bmatrix} \phi_1 \\ \phi_2 \end{bmatrix} = \boldsymbol{\phi} + \boldsymbol{F}(\beta)\boldsymbol{\phi}.$$

Using now definition (13) allows us to write $\beta = \beta_d(\boldsymbol{\phi}) - e_d$ and consequently $\boldsymbol{v} = \boldsymbol{\phi} + \boldsymbol{F}(e_d, \beta_d(\boldsymbol{\phi}))\boldsymbol{\phi} = \boldsymbol{\phi} + \boldsymbol{\epsilon}(e_d, \boldsymbol{\phi})$.

Next, we show that $\boldsymbol{\epsilon}(e_d = 0, \boldsymbol{\phi}) = \mathbf{0}$. For $e_d = 0$ and using Eq. (10) or Eq. (20), one obtains

$$\begin{bmatrix} \epsilon_1(e_d = 0, \boldsymbol{\phi}) \\ \epsilon_2(e_d = 0, \boldsymbol{\phi}) \end{bmatrix} = \begin{bmatrix} -\phi_1 \mathrm{c}^2\beta_d + \frac{1}{L}\big(L\phi_1\mathrm{c}\beta_d\big)\mathrm{c}\beta_d \\ L\mathrm{s}\beta_d\big(\frac{1}{L}\phi_2\mathrm{s}\beta_d\big) - \phi_2\mathrm{s}^2\beta_d \end{bmatrix} = \begin{bmatrix} 0 \\ 0 \end{bmatrix},$$

where the argument $\boldsymbol{\phi}$ of β_d has been omitted for compactness.

Acknowledgments

This work was supported in part by the Polish scientific fund in years 2010–2012 as the research project No. N N514 087038.

References

1. M. Aicardi, G. Casalino, A. Bicchi and A. Balestrino, "Closed loop steering of unicycle-like vehicles via Lyapunov techniques," *IEEE Robot. Autom. Mag.* **2**, 27–35 (1995).
2. J. Angeles, "An innovative drive for wheeled mobile robots," *IEEE/ASME Trans. Mechatronics* **10**(1), 43–49. (2005).
3. A. Astolfi, "Exponential Stabilization of a Car-like Vehicle," *Proceedings of the IEEE International Conference on Robotics and Automation*, Nagoya, Aichi, Japan (1995) pp. 1391–1396.
4. A. Astolfi, "Exponential Stabilization of a Wheeled Mobile Robot via Discontinuous Control," *Proceedings of the Nonlinear Control System Design Symposium*, Lake Tahoe, USA (1995) pp. 741–746.
5. S. P. Bhat and D. S. Bernstein, "Finite-time stability of continuous autonomous systems," *SIAM J. Control Optim.* **38**(3), 751–766 (2000).
6. C. Canudas de Wit, H. Khennouf, C. Samson and O. J. Sordalen, "Nonlinear Control Design for Mobile Robots," **In**: *Recent Trends in Mobile Robots* (Y. F. Zheng, ed.) (World Scientific, Singapore, 1993) vol. 11, chapter 5, pp. 121–156.
7. A. Cherubini, F. Chaumette and G. Oriolo, "Visual servoing for path reaching with nonholonomic robots," *Robotica*. Available on CJO 2011, doi: 10.1017/S0263574711000221.
8. M. L. Corradini and G. Orlando, "Control of mobile robots with uncertainties in the dynamical model: A discrete time sliding mode approach with experimental results," *Control Eng. Pract.* **10**, 23–34 (2002).
9. B. d'Andrea Novel, G. Campion and G. Bastin, "Control of nonholonomic wheeled mobile robots by state feedback linearization," *Int. J. Robot. Res.* **14**, 543–559 (1995).
10. C. Canudas de Wit, B. Siciliano and G. Bastin, *Theory of Robot Control* (Springer-Verlag, New York, 1996).
11. W. E. Dixon, D. M. Dawson, E. Zergeroglu and A. Behal, *Nonlinear Control of Wheeled Mobile Robots* (Springer, London, 2001).
12. F. Gomez-Bravo, F. Cuesta and A. Ollero, "Parallel and diagonal parking in nonholonomic autonomous vehicles,". *Eng. Appl. Artif. Intell.* **14**, 419–434 (2001).
13. R. Gonzalez, M. Fiacchini, T. Alamo, J. L. Guzman and F. Rodriguez, "Adaptive control for a mobile robot under slip conditions using an LMI-based approach," *Eur. J. Control* **16**(2), 144–155 (2010).
14. H. K. Khalil, *Nonlinear Systems*, 3rd ed. (Prentice-Hall, Upper Saddle River, New Jersey, 2002).
15. B. M. Kim and P. Tsiotras, "Controllers for unicycle-type wheeled robots: theoretical results and experimental validation," *IEEE Trans. Robot. Autom.* **18**(3), 294–307 (2002).
16. E. Lefeber and H. Nijmeijer, "Adaptive Tracking Control of Nonholonomic Systems: An Example," *Proceedings of the 38th Conference on Decision and Control*, Phoenix, USA (1999) pp. 2094–2099.
17. A. De Luca and G. Oriolo, "Modeling and Control of Nonholonomic Mechanical Systems," **In**: *Kinematics and Dynamics of Multi-Body Systems* (J. Angeles and A. Kecskementhy, eds.) (Springer-Verlag, Wien, 1995) chapter 7, pp. 277–342.
18. A. De Luca, G. Oriolo and C. Samson, "Feedback Control of a Nonholonomic Car-Like Robot," **In**: *Robot Motion Planning and Control* (J. P. Laumond, ed.) (Springer-Verlag, New York, Inc., 1998) chapter 4, pp. 170–253.
19. M. Michalek and K. Kozlowski, "Vector-field-orientation feedback control method for a differentially driven vehicle," *IEEE Trans. Control Syst. Technol.* **18**(1), 45–65 (2010).
20. P. Morin and C. Samson, "Trajectory Tracking for Non-Holonomic Vehicles: Overview and Case Study," *Proceedings of the 4th International Workshop On Robot Motion and Control*, Puszczykowo, Poland (2004) pp. 139–153.
21. P. Morin and C. Samson, "Trajectory Tracking for Nonholonomic Vehicles," **In:** *Robot Motion and Control. Recent Developments*, Lecture Notes in Control and Information Sciences (Springer, 2006) vol. 335, pp. 3–23.
22. P. Morin and C. Samson, "Motion Control of Wheeled Mobile Robots," **In**: *Springer Handbook of Robotics* (B. Siciliano and O. Khatib, eds.) (Springer, 2008) pp. 799–826.
23. P. Morin and C. Samson, "Control of nonholonomic mobile robots based on the transverse function approach," *IEEE Trans. Robot.* **25**(5), 1058–1073 (2009).
24. G. Oriolo, A. De Luca and M. Venditteli, "WMR control via dynamic feedback linearization: Design, implementation and experimental validation," *IEEE Trans. Control Syst. Technol.* **10**, 835–852 (2002).
25. J. B. Pomet, "Explicit design of time varying stabilization control laws for a class of controllable systems without drifts," *Syst. Control Lett.* **18**, 147–158 (1992).
26. A. Rosales, G. Scaglia, V. Mut and F. di Sciascio, "Trajectory tracking of mobile robots in dynamic environments—A linear algebra approach," *Robotica* **27**, 981–997 (2009).
27. C. Samson, "Path Following and Time-varying Feedback Stabilization of a Wheeled Mobile Robot," *Proceedings of the International Conference (ICARCV '92)*, Singapur (1992) pp. 13.1.1–13.1.5.
28. C. Samson, "Time-varying feedback stabilization of car-like wheeled mobile robots," *Int. J. Robot. Res.* **12**, 55–64 (1993).
29. C. Samson, "Control of chained systems; application to path following and time-varying point-stabilization of mobile robots," *IEEE Trans. Autom. Control* **40**, 64–77 (1995).
30. R. Siegwart and I. R. Nourbakhsh, *Introduction to Autonomous Mobile Robots* (The MIT Press, 2004).
31. O. J. Sørdalen and O. Egeland, "Exponential stabilization of nonholonomic chained systems," *IEEE Trans. Autom. Control* **40**(1), 35–49 (1995).
32. O. J. Sordalen and C. Canudas de Wit, "Exponential control law for a mobile robot: Extention to path following," *IEEE Trans. Robot. Autom.* **9**(6), 837–842 (1993).
33. H. Teimoori and A. V. Savkin, "A biologically inspired method for robot navigation in a cluttered environment," *Robotica* **28**, 637–648 (2010).
34. J. M. Toibero F. Roberti and R. Carelli, "Stable contour-following control of wheeled mobile robots" *Robotica* **27**, 1–12 (2009).

35. D. Wang and G. Xu "Full-state tracking and internal dynamics of nonholonomic wheeled mobile robots," *IEEE Trans. Mechatronics* **8**(2), 203–214 (2003).
36. M. Werling and L. Gröll, "Low-Level Controllers Realizing high-Level Decisions in an Autonomous Vehicle," *Proceedings of the 2008 IEEE Intelligent Vehicles Symposium*, Eindhoven, The Netherlands (2008) pp. 1113–1118.
37. M. Werling, L. Gröll and G. Bretthauer, "Invariant trajectory tracking with a full-size autonomous road vehicle," *IEEE Trans. Robot.* **26**(4), 758–765 (2010).
38. J. Yi, D. Song, A. Levandowski and S. Jayasuriya, "Trajectory Tracking and Balance Stabilization Control of Autonomous Motorcycles," *Proceedings of the 2006 IEEE International Conference on Robotics and Automation*, Orlando, USA (2006) pp. 2583–2588.